# Spectra and statistics in compressible isotropic turbulence

Jianchun Wang,* Toshiyuki Gotoh, and Takeshi Watanabe
*Department of Physical Science and Engineering, Nagoya Institute of Technology, Nagoya 466-8555, Japan*
(Received 3 August 2016; published 27 January 2017)

Spectra and one-point statistics of velocity and thermodynamic variables in isotropic turbulence of compressible fluid are examined by using numerical simulations with solenoidal forcing at the turbulent Mach number $M_t$ from 0.05 to 1.0 and at the Taylor Reynolds number $\mathrm{Re}_\lambda$ from 40 to 350. The velocity field is decomposed into a solenoidal component and a compressible component in terms of the Helmholtz decomposition, and the compressible velocity component is further decomposed into a pseudosound component, namely, the hydrodynamic component associated with the incompressible field and an acoustic component associated with sound waves. It is found that the acoustic mode dominates over the pseudosound mode at turbulent Mach numbers $M_t \geqslant 0.4$ in our numerical simulations. At turbulent Mach numbers $M_t \leqslant 0.4$, there exists a critical wave number $k_c$ beyond which the pseudosound mode dominates while the acoustic mode dominates at small wave numbers $k < k_c$. In the pseudosound-mode-dominated region, the compressible velocity is fully enslaved to the solenoidal velocity, and its spectrum scales as $M_t^4 k^{-3}$ in the inertial range. It is also found that in the inertial range, the spectra of pressure, density, and temperature exhibit a $k^{-7/3}$ scaling for $M_t \leqslant 0.3$ and a $k^{-5/3}$ scaling for $M_t \geqslant 0.5$.

DOI: 10.1103/PhysRevFluids.2.013403

## I. INTRODUCTION

Compressible turbulence is of great significance in a number of areas of scientific and industrial interest, including acoustic phenomena, designs of subsonic and supersonic aircrafts, solar wind, and star-forming clouds in astrophysics. A deeper understanding of the statistics and structures of compressible turbulence is also crucial to the development of suitable subgrid-scale models for large eddy simulation of complex compressible turbulent flows. The velocity dynamics in compressible turbulence includes compression and expansion in addition to multiscale shear and eddy motions and thus is more complex than that of incompressible turbulence [1–10]. Moreover, in compressible turbulence, there are nonlinear couplings between the velocity and thermodynamic variables such as density, pressure, and temperature.

Unlike incompressible turbulence, there is an extra nondimensional parameter, the turbulent Mach number, other than the Reynolds numbers in compressible turbulence. In this paper, we focus on the statistical properties of compressible isotropic turbulence at low Mach numbers. Kovasznay [11] proposed a small parameter expansion for small turbulent fluctuations with respect to a uniform mean flow and decomposed the turbulent flow of the compressible fluid into three components, namely, the vorticity, acoustic, and entropy modes, under the assumption of weak compressibility. However, the Kovasznay decomposition is limited to linear problems. For nonlinear problems such as fully developed turbulence, the Helmholtz decomposition is useful to separate the velocity field into solenoidal and compressible modes [1,3,9]. Correspondingly, the pressure can also be decomposed into two parts, the incompressible and compressible parts, the former being defined as the one through the Poisson equation in the incompressible turbulence [1,9] and the latter owing to the

*jwang.pku@gmail.com

 

compressible velocity. For turbulent Mach numbers $M_t$ up to 1.0, the spectrum and one-point statistics of the solenoidal component of the flow have been found to be similar to those of incompressible turbulence [12–15].

For low turbulent Mach numbers, two scenarios for the Mach number scaling of the compressible component have been suggested: an acoustic scenario suggested by Sarkar *et al.* [16] and a pseudosound scenario suggested by Ristorcelli [17]. Sarkar *et al.* [16] pointed out that in weakly compressible homogeneous turbulence, the compressible component quickly attains a quasiequilibrium state, because the compressible mode has a short time scale relative to that of the incompressible mode. They derived an equipartition relation between the kinetic energy and the potential energy of the compressible components and verified it by direct numerical simulation (DNS) of the compressible isotropic decaying turbulence. Ristorcelli [17] pointed out that by applying the pseudosound theory (at the inner scale that is much smaller than the typical wave length of sound waves), the fluid behaves as if it were incompressible. The compressible component of the velocity field can be fully determined through the solenoidal components of velocity and pressure. Moreover, he derived the representations for the pressure dilatation and dilatational dissipation in one-point moment closures for compressible turbulence, from the pseudosound relationship. Our understanding, however, is still limited as to which scenario is realized and what conditions should be satisfied for their realization.

The aim of this paper is to examine the above two scenarios and to explore the condition in which one or both of the two scenarios is realized, by using the spectrum and the one-point statistics of the compressible component of velocity. For this purpose, it is necessary to introduce a method that explicitly decomposes the compressible field into a pseudosound component and an acoustic component, because the Helmholtz decomposition alone cannot distinguish between the acoustic waves [18] and other compressible phenomena [1]. As we will see in the case of the latter, it is found from a set of large-scale DNSs and theoretical analysis that for fully developed weakly compressible turbulence both scenarios can coexist but in different ranges of wave numbers.

In the early phase of studies of the compressible turbulence by DNS, there are many interesting works in addition to those mentioned in previous paragraphs: the growth of the root mean square (rms) values of the compressible components of velocity [19], the Mach number effects on the velocity spectrum [20], the mechanism for the exchange of kinetic energy and internal energy [21], temporal correlations of both solenoidal and compressible components of velocity [22], etc. Large-scale DNSs of the compressible isotropic turbulence have recently been performed at grid resolutions as high as $1024^3$ [14,15,23] and $2048^3$ [9,24], which allowed us to explore the asymptotic power-law scaling of the kinetic energy spectrum. It was reported that the spectrum of velocity exhibits a $k^{-5/3}$ scaling in the inertial range at a turbulent Mach number up to 1.0 [14,23,24]. Donzis and Jagannathan [24] computed the spectrum of the compressible velocity component at $M_t \approx 0.1$, 0.3, and 0.6 for the Taylor Reynolds numbers $\mathrm{Re}_\lambda \approx 170$, 430, and 170 respectively. Although the width of the inertial range observed in the DNS was very short, they reported that the spectra of density, pressure, and temperature were consistent with a $k^{-5/3}$ inertial range scaling at relatively low Taylor Reynolds numbers. They also pointed out that the pressure spectrum may also be consistent with $k^{-7/3}$ at sufficiently low turbulent Mach numbers. Higher Reynolds numbers are necessary to unambiguously determine the inertial range scaling of the pressure spectrum in compressible turbulence [24].

Besides numerical studies, theoretical efforts using the spectral theory of turbulence have also been devoted to find the spectra of velocity and pressure in compressible turbulence. Bataille *et al.* [25] reported that the spectrum of the compressible velocity component obeys a $k^{-11/3}$ scaling in the inertial range at low to moderate turbulent Mach numbers by numerically solving an eddy-damped-quasinormal-Markovian (EDQNM) model. They also found that the kinetic energy transfer of the compressible component is much smaller than that of the solenoidal component. Bertoglio *et al.* [26] extended both the direct interaction approximation (DIA) and EDQNM model to weakly compressible turbulence. Their EDQNM model showed that at low Mach numbers the spectra of the compressible components of the velocity and pressure have a $k^{-11/3}$ scaling in the

inertial range. Fauchet and Bertoglio [27] developed an improved EDQNM model and found that the spectrum of the compressible velocity component exhibits a $M_t^4 k^{-3}$ scaling in the inertial range.

There seems less consensus on the wave-number scaling of the various spectra in the inertial ranges that may vary with the Mach number. In this paper, we examine the wave-number scaling of spectra for both the velocity and thermodynamic quantities in terms of the large-scale DNS. The rest of the paper is organized as follows. Section II briefly describes the governing equations of compressible turbulence. Section III introduces a decomposition: The compressible components of velocity and pressure can be decomposed into pseudosound and acoustic components. Section IV describes the numerical methods and parameters. Sections V and VI investigate the spectra and one-point statistics of velocity and thermodynamic variables by numerical simulations. The summary and the conclusion will be presented in Sec. VII.

## II. GOVERNING EQUATIONS OF COMPRESSIBLE TURBULENCE

We consider compressible turbulence governed by the following dimensionless Navier-Stokes equations [3,14]:

$$\frac{\partial \rho}{\partial t} + \frac{\partial(\rho u_j)}{\partial x_j} = 0, \tag{1}$$

$$\frac{\partial(\rho u_i)}{\partial t} + \frac{\partial[\rho u_i u_j + p\delta_{ij}]}{\partial x_j} = \frac{1}{\mathrm{Re}}\frac{\partial \sigma_{ij}}{\partial x_j} + \mathcal{F}_i, \tag{2}$$

$$\frac{\partial \mathcal{E}}{\partial t} + \frac{\partial[(\mathcal{E}+p)u_j]}{\partial x_j} = \frac{1}{\alpha}\frac{\partial}{\partial x_j}\left(\kappa\frac{\partial T}{\partial x_j}\right) + \frac{1}{\mathrm{Re}}\frac{\partial(\sigma_{ij}u_i)}{\partial x_j} - \Lambda + \mathcal{F}_j u_j, \tag{3}$$

$$p = \rho T/(\gamma M^2), \tag{4}$$

where $\rho$ is the density, $u_i$ is the velocity component, $p$ is the pressure, and $T$ is the temperature. The viscous stress $\sigma_{ij}$ is given by

$$\sigma_{ij} = \mu\left(\frac{\partial u_i}{\partial x_j} + \frac{\partial u_j}{\partial x_i}\right) - \frac{2}{3}\mu\theta\delta_{ij}, \tag{5}$$

and the total energy per unit volume $\mathcal{E}$ is given by

$$\mathcal{E} = \frac{p}{\gamma - 1} + \frac{1}{2}\rho(u_j u_j). \tag{6}$$

Here, we denote $\mathcal{F}_i$ as the dimensionless, large-scale force per unit volume to the fluid momentum and $\Lambda$ as the dimensionless large-scale cooling function per unit volume. $\theta \equiv \partial u_k/\partial x_k$ is the normalized velocity divergence.

In the governing equations, we have normalized each variable by a reference length $L_f$, velocity $U_f$, density $\rho_f$, temperature $T_f$, energy per unit volume $\rho_f U_f^2$, viscosity $\mu_f$, and thermal conductivity $\kappa_f$. Pressure is normalized by $\rho_f U_f^2$. The three reference governing parameters are the reference Reynolds number $\mathrm{Re} \equiv \rho_f U_f L_f/\mu_f$, the reference Mach number $M = U_f/c_f$, and the reference Prandtl number $\mathrm{Pr} \equiv \mu_f C_p/\kappa_f$. Here, the speed of sound is defined by $c_f \equiv \sqrt{\gamma R T_f}$. $\gamma \equiv C_p/C_v$ is the ratio of specific heat at constant pressure $C_p$ to that at constant volume $C_v$ and is assumed to be equal to 1.4. $R$ is the specific gas constant. The parameter $\alpha$ is given by $\alpha \equiv \mathrm{Pr}\,\mathrm{Re}(\gamma - 1)M^2$. The parameter Pr is assumed to be equal to 0.7.

The temperature-dependent viscosity coefficient and thermal conductivity coefficient is specified by Sutherland's law [28]. The Taylor microscale Reynolds number $\mathrm{Re}_\lambda$ and the turbulent Mach number $M_t$ are defined respectively by [13]

$$\mathrm{Re}_\lambda = \mathrm{Re}\frac{\langle\rho\rangle u'\lambda}{\sqrt{3}\langle\mu\rangle}, \quad M_t = M\frac{u'}{\langle\sqrt{T}\rangle}, \tag{7}$$

where $\langle\rangle$ stands for ensemble average. Here, the root mean square value of the velocity magnitude is defined by $u' = \sqrt{\langle u_1^2 + u_2^2 + u_3^2\rangle}$ and the Taylor microscale is defined by

$$\lambda = \sqrt{\frac{\langle u_1^2 + u_2^2 + u_3^2\rangle}{\langle (\partial u_1/\partial x_1)^2 + (\partial u_2/\partial x_2)^2 + (\partial u_3/\partial x_3)^2\rangle}}. \tag{8}$$

## III. DECOMPOSITION: PSEUDOSOUND MODE AND ACOUSTIC MODE

Each thermodynamic variable can be decomposed into a mean (ensemble averaging) value and a fluctuating value, namely, $\rho = \rho_0 + \rho'$, $p = p_0 + p'$, and $T = T_0 + T'$. Here, the prime stands for the fluctuating value. The mean values of three thermodynamic variables are $\rho_0 = 1$, $p_0 = 1/(\gamma M^2)$, and $T_0 \approx 1$, respectively in our numerical simulations. We apply the Helmholtz decomposition to the velocity field $\boldsymbol{u}$ [1,3,9,14]: $\boldsymbol{u} = \boldsymbol{u}^s + \boldsymbol{u}^c$, where the solenoidal component $\boldsymbol{u}^s$ and compressible component $\boldsymbol{u}^c$ satisfy conditions $\partial u_i^s/\partial x_i = 0$ and $\epsilon_{ijk}\partial u_j^c/\partial x_k = 0$, respectively. The kinetic energy of each component of the velocity is defined by $K^s = \langle[(u_1^s)^2 + (u_2^s)^2 + (u_3^s)^2]/2\rangle$ and $K^c = \langle[(u_1^c)^2 + (u_2^c)^2 + (u_3^c)^2]/2\rangle$, respectively. At a small turbulent Mach number ($M_t \ll 1$), the ratio of the compressible kinetic energy to the solenoidal kinetic energy is much smaller than 1: $K^c/K^s \ll 1$. The magnitudes of fluctuations of thermodynamic variables are also much smaller than their mean values: $\rho' \ll 1$, $p' \ll 1/(\gamma M^2)$, and $T' \ll 1$. Thus, we have the following approximations:

$$\rho \approx \rho_0, \tag{9}$$

$$p \approx p_0, \tag{10}$$

and

$$\boldsymbol{u} \approx \boldsymbol{u}^s. \tag{11}$$

According to the definition of velocity decomposition, we have the following relation:

$$\boldsymbol{\nabla}\cdot\boldsymbol{u} = \boldsymbol{\nabla}\cdot\boldsymbol{u}^c. \tag{12}$$

In the case of a very small turbulent Mach number, we also have the following approximations:

$$\frac{1}{\rho} - \frac{1}{\rho_0} \approx -\frac{\rho'}{\rho_0^2}, \tag{13}$$

and

$$\boldsymbol{u}\cdot\boldsymbol{\nabla}\boldsymbol{u} - \boldsymbol{u}^s\cdot\boldsymbol{\nabla}\boldsymbol{u}^s \approx \boldsymbol{u}^c\cdot\boldsymbol{\nabla}\boldsymbol{u}^s + \boldsymbol{u}^s\cdot\boldsymbol{\nabla}\boldsymbol{u}^c. \tag{14}$$

The fluctuating pressure $p'$ can be decomposed into a solenoidal pressure $p^s$ and a compressible pressure $p^c$ [1,9]: $p' = p^s + p^c$, where the solenoidal pressure satisfies the Poisson equation,

$$\nabla^2 p^s = -\rho_0 \frac{\partial u_i^s}{\partial x_j}\frac{\partial u_j^s}{\partial x_i}. \tag{15}$$

We consider the inviscid dynamical equations of density, velocity, and pressure as studied by Ristorcelli [17]:

$$\frac{\partial \rho}{\partial t} + u_j\frac{\partial \rho}{\partial x_j} = -\rho\frac{\partial u_j}{\partial x_j}, \tag{16}$$

$$\frac{\partial u_i}{\partial t} + u_j\frac{\partial u_i}{\partial x_j} = -\frac{1}{\rho}\frac{\partial p}{\partial x_i} + f_i, \tag{17}$$

and

$$\frac{\partial p}{\partial t} + u_j\frac{\partial p}{\partial x_j} = -\gamma p\frac{\partial u_j}{\partial x_j}, \tag{18}$$

where $f_i$ is assumed to be solenoidal. The effects of neglected dissipative terms are only significant at relatively small scales [17,29].

We have the following exact relations for the solenoidal components of velocity and pressure:

$$\frac{\partial u_j^s}{\partial x_j} = 0 \tag{19}$$

and

$$\Pi\left\{u_j^s \frac{\partial u_i^s}{\partial x_j}\right\} = -\frac{1}{\rho_0}\frac{\partial p^s}{\partial x_i}, \tag{20}$$

where $\Pi \equiv \mathcal{I} - \mathcal{P}$. Here, $\mathcal{I}$ is the identity operator and $\mathcal{P}$ is the projection operator: $\mathcal{P}\boldsymbol{g} \equiv \boldsymbol{g} - \boldsymbol{\nabla}\nabla^{-2}\boldsymbol{\nabla}\cdot\boldsymbol{g}$. Thus, $\Pi\boldsymbol{g} = \boldsymbol{\nabla}\nabla^{-2}\boldsymbol{\nabla}\cdot\boldsymbol{g}$. After applying the projection operator $\mathcal{P}$ to the velocity equation, we obtain

$$\frac{\partial u_i^s}{\partial t} + \mathcal{P}\left\{u_j^s \frac{\partial u_i^s}{\partial x_j}\right\} = f_i. \tag{21}$$

After applying the relations (9)–(12), we obtain the equations for the fluctuations of density and pressure:

$$\frac{\partial \rho'}{\partial t} + u_j^s \frac{\partial \rho'}{\partial x_j} \approx -\rho_0 \frac{\partial u_j^c}{\partial x_j} \tag{22}$$

and

$$\frac{\partial p'}{\partial t} + u_j^s \frac{\partial p'}{\partial x_j} \approx -\gamma p_0 \frac{\partial u_j^c}{\partial x_j}. \tag{23}$$

The equation of the compressible velocity component can be obtained by applying the operator $\Pi$ to the velocity equation as

$$\frac{\partial u_i^c}{\partial t} + \Pi\left\{u_j^s \frac{\partial u_i^c}{\partial x_j} + u_j^c \frac{\partial u_i^s}{\partial x_j}\right\} \approx -\frac{1}{\rho_0}\frac{\partial p^c}{\partial x_i} + \Pi\left\{\frac{\rho'}{\rho_0^2}\frac{\partial p'}{\partial x_i}\right\}. \tag{24}$$

To obtain Eq. (24), we extracted both $\Pi\{u_j^s \frac{\partial u_i^s}{\partial x_j}\}$ and $-\frac{1}{\rho_0}\frac{\partial p^s}{\partial x_i}$ terms according to Eq. (20). Here, we also used the approximation relations (13) and (14).

We assume that the fluid is nearly isentropic so that the density and pressure are related as $\rho' \approx \rho_0 p'/\gamma p_0$. Then we obtain

$$\Pi\left\{\frac{\rho'}{\rho_0^2}\frac{\partial p'}{\partial x_i}\right\} \approx \frac{1}{2\gamma p_0 \rho_0}\frac{\partial p'^2}{\partial x_i}. \tag{25}$$

We show the updated equations for the compressible velocity and compressible pressure as follows:

$$\frac{\partial u_i^c}{\partial t} + \Pi\left\{u_j^s \frac{\partial u_i^c}{\partial x_j} + u_j^c \frac{\partial u_i^s}{\partial x_j}\right\} \approx -\frac{1}{\rho_0}\frac{\partial p^c}{\partial x_i} + \frac{1}{2\gamma p_0 \rho_0}\frac{\partial p'^2}{\partial x_i} \tag{26}$$

and

$$\frac{\partial p^c}{\partial t} + u_j^s \frac{\partial p^c}{\partial x_j} \approx -\gamma p_0 \frac{\partial u_j^c}{\partial x_j} - \left(\frac{\partial p^s}{\partial t} + u_j^s \frac{\partial p^s}{\partial x_j}\right). \tag{27}$$

It is worth noting that Eqs. (26) and (27) governing the compressible components of velocity and pressure are valid under the assumption of a small turbulent Mach number, including both the pseudosound scenario [17] and acoustic scenario [16] of weakly compressible turbulence. Here, we propose the following scenario for solenoidally forced stationary weakly compressible turbulence

in a cubic box: (1) At a given Taylor Reynolds number, as the turbulent Mach number becomes infinitesimal, the flow is dominated by the pseudosound relationship; and (2) generally, for the fully developed turbulence at a large enough Taylor Reynolds number, there exists a critical length scale $l_c(M_t)$ that depends on the turbulent Mach number. The pseudosound relationship is valid at small scales $l < l_c$ and the acoustic relationship is valid at large scales $l > l_c$. The idea that acoustic modes usually dominate at large scales is not new and can be found in previous studies on the acoustic waves generated by turbulence [30–32]. An improved EDQNM model by Fauchet and Bertoglio [27] also indicates that acoustic modes dominate at large scales and pseudosound modes dominate at smaller scales. Here, we will study the critical condition for the transition between two types of modes and the effect of the transition on the statistics of isotropic turbulence.

Now, we remind the reader briefly of the pseudosound relationship [17]. The pseudosound theory was originally developed for compressible flow in the near field of a compact acoustic source [17]. The fluid behaves as if it were incompressible. The dynamics of the compressible velocity and compressible pressure are fully determined by incompressible velocity. According to the pseudosound relationship [17], we have

$$\boldsymbol{u}^c \sim M_t^2 \boldsymbol{u}^s \ll \boldsymbol{u}^s, \tag{28}$$

$$p^c \sim M_t^2 p^s \ll p^s. \tag{29}$$

By noting that $p_0 = O[(\gamma M^2)^{-1}]$, we obtain the following approximations for $\boldsymbol{u}^c$ and $p^c$ from Eqs. (26) and (27):

$$\gamma p_0 \frac{\partial u_j^c}{\partial x_j} \approx -\left(\frac{\partial p^s}{\partial t} + u_j^s \frac{\partial p^s}{\partial x_j}\right), \tag{30}$$

$$\frac{1}{\rho_0}\frac{\partial p^c}{\partial x_i} \approx -\left(\frac{\partial u_i^c}{\partial t} + \Pi\left\{u_j^s \frac{\partial u_i^c}{\partial x_j} + u_j^c \frac{\partial u_i^s}{\partial x_j}\right\}\right) + \frac{1}{2\gamma p_0 \rho_0}\frac{\partial (p^s)^2}{\partial x_i}. \tag{31}$$

However, here we consider the stationary compressible turbulence in a cubic box, which is different from the compressible flow in the near field of a compact acoustic source. We need to investigate the validity of this relationship. Thus, we propose a type of decomposition for the compressible velocity and compressible pressure: $\boldsymbol{u}^c = \boldsymbol{u}^{cs} + \boldsymbol{u}^{cc}$ and $p^c = p^{cs} + p^{cc}$. Here, $\boldsymbol{u}^{cs}$ and $p^{cs}$ are the pseudosound components of velocity and pressure. $\boldsymbol{u}^{cc}$ and $p^{cc}$ are the acoustic components of velocity and pressure, whose magnitudes signify the deviation of compressible turbulence from the pseudosound relationship.

The pseudosound components of velocity and pressure are governed by Eqs. (30) and (31):

$$\gamma p_0 \frac{\partial u_j^{cs}}{\partial x_j} = -\left(\frac{\partial p^s}{\partial t} + u_j^s \frac{\partial p^s}{\partial x_j}\right), \tag{32}$$

$$\frac{1}{\rho_0}\frac{\partial p^{cs}}{\partial x_i} = -\left(\frac{\partial u_i^{cs}}{\partial t} + \Pi\left\{u_j^s \frac{\partial u_i^{cs}}{\partial x_j} + u_j^{cs} \frac{\partial u_i^s}{\partial x_j}\right\}\right) + \frac{1}{2\gamma p_0 \rho_0}\frac{\partial (p^s)^2}{\partial x_i}. \tag{33}$$

To be clearer, the pseudosound velocity and pressure are determined by incompressible velocity in the following manner:

$$\boldsymbol{u}^{cs} = -\frac{1}{\gamma p_0}\nabla\nabla^{-2}\left(\frac{\partial p^s}{\partial t} + \boldsymbol{u}^s \cdot \nabla p^s\right), \tag{34}$$

$$p^{cs} = \frac{(p^s)^2}{2\gamma p_0} - \rho_0 \nabla^{-2}\nabla \cdot \left(\frac{\partial \boldsymbol{u}^{cs}}{\partial t} + \boldsymbol{u}^s \cdot \nabla \boldsymbol{u}^{cs} + \boldsymbol{u}^{cs} \cdot \nabla \boldsymbol{u}^s\right). \tag{35}$$

We define the energy $K^{cs}$ of the pseudosound velocity and the variance $K_p^{cs}$ of the pseudosound pressure, respectively, by $K^{cs} = \langle(\mathbf{u}^{cs})^2/2\rangle$ and $K_p^{cs} = \langle(p^{cs})^2\rangle$. It is easily found from the order estimates (28) and (29) that $K^{cs}/K^s \sim O(M_t^4)$ and $K_p^{cs}/K_p^s \sim O(M_t^4)$.

Let us consider the spectra of the pseudosound components of velocity and pressure: $E^{cs}(k)$ and $E_p^{cs}(k)$, where $\int_0^\infty E^{cs}(k)dk = \langle(\mathbf{u}^{cs})^2\rangle/2$ and $\int_0^\infty E_p^{cs}(k)dk = \langle(p^{cs})^2\rangle$. It is worth noting that the dimension of $p^s/\rho_0$ is the same as the dimension of $(\mathbf{u}^s)^2$. Specifically, according to the dimensional analysis method, we denote the characteristic time scale as $\tau_k$ at wave number $k$. The normalized solenoidal pressure at wave number $k$ satisfies the relation: $p_k^s/\rho_0 \sim 1/(k^2\tau_k^2)$. The normalized pseudosound component of velocity at wave number $k$ satisfies the relation $u_k^{cs}\, p_0/\rho_0 \sim p^s/(\rho_0 k\tau_k) \sim 1/(k^3\tau_k^3)$. The spectrum of the pseudosound component of velocity satisfies the relation $E^{cs}(k) \sim (u_k^{cs})^2/k \sim \rho_0^2/p_0^2/(k^7\tau_k^6)$. It is worth noting that the characteristic time scale $\tau_k$ satisfies the relation $\tau_k \sim \epsilon^{-1/3}k^{-2/3}$ [33–35], for wave number $k$ in the inertial range, where $\epsilon$ is the dissipation rate of velocity. Thus, we obtain $E^{cs}(k) \sim \rho_0^2/p_0^2\epsilon^2k^{-3}$ in the inertial range. Similarly, we obtain $E_p^{cs}(k) \sim (p_k^{cs})^2/k \sim \rho_0^4/p_0^2/(k^9\tau_k^8)$ and $E_p^{cs}(k) \sim \rho_0^4/p_0^2\epsilon^{8/3}k^{-11/3}$ in the inertial range.

We also notice the relation $\rho_0^2/p_0^2 \sim M_t^4/(u')^4 \sim M_t^4/(L_I\epsilon)^{4/3}$, where $L_I$ is the integral length scale of velocity. Thus, we obtain new formulations for the inertial scaling behaviors of the spectra $E^{cs}(k)$ and $E_p^{cs}(k)$ as

$$E^{cs}(k) = C_v^{PS} M_t^4 L_I^{-4/3}\epsilon^{2/3}k^{-3}, \tag{36}$$

$$E_p^{cs}(k) = C_p^{PS}\rho_0^2 M_t^4 L_I^{-4/3}\epsilon^{4/3}k^{-11/3}. \tag{37}$$

Thus, in the pseudosound-mode-dominated regime, the spectra of the compressible velocity and compressible pressure are expected to obey the following scaling behaviors in the inertial range

$$E^c(k) \sim M_t^4 k^{-3}, \tag{38}$$

$$E_p^c(k) \sim M_t^4 k^{-11/3}. \tag{39}$$

Our theoretical relations (38) and (39) based on the pseudosound theory [17] are consistent with those of an improved EDQNM closure model developed by Fauchet and Bertoglio [1,27].

## IV. NUMERICAL METHOD AND SYSTEM PARAMETERS

The governing equations of compressible turbulence are solved in conservative form in a cubic box with side lengths $2\pi$, by using periodic boundary conditions in all three spatial directions. For numerical method, we apply the eighth-order central compact finite difference scheme [36] for weakly compressible turbulence, where $M_t \leqslant 0.4$, and apply a hybrid compact-weighted essentially nonoscillatory (compact-WENO) scheme [28] for moderately and highly compressible turbulence, where $M_t \geqslant 0.5$. The hybrid scheme combines the eighth-order central compact finite difference scheme [36] for smooth regions and the seventh-order WENO scheme [37] for shock regions. Some grid refinement studies of the hybrid scheme for a turbulent Mach number of approximately 1.0 were performed in previous works [13,14].

The velocity field is forced by fixing the energy spectrum within the two lowest wave-number shells. The force is applied only to the solenoidal component of the velocity field. A spatially uniform thermal cooling $\Lambda$ is employed to sustain the internal energy in a statistically steady state. The magnitude of thermal cooling is set according to the constraint that the internal energy equals a constant [28].

We summarize the overall parameters of all the simulations in Tables I–III. The Kolmogorov length scale is defined by $\eta = [\langle\mu/(\mathrm{Re}\rho)\rangle^3/\epsilon]^{1/4}$, where the dissipation rate per unit mass is given by $\epsilon = \langle\sigma_{ij}S_{ij}/(\mathrm{Re}\rho)\rangle$. The strain rate tensor $S_{ij}$ is defined by $S_{ij} = \frac{1}{2}(\frac{\partial u_i}{\partial x_j} + \frac{\partial u_j}{\partial x_i})$. The magnitude of Kolmogorov length scale $\eta$ represents the dissipation-range resolution, which plays a significant role in the grid convergence of velocity statistics in DNS [38]. We show that the resolution parameter $\eta/\Delta x$ is in the range $0.58 < \eta/\Delta x < 1.05$ in our simulations, where $\Delta x$ denotes the gridding length

TABLE I. Simulation parameters and resulting flow statistics for $64^3$ and $128^3$ grid resolutions.

| Resolution | $\mathrm{Re}_\lambda$ | $M_t$ | $\eta/\Delta x$ | $L_I/\eta$ | $\lambda/\eta$ | $S_3$ | $D=\epsilon L_I/(u'/\sqrt{3})^3$ |
|---|---|---|---|---|---|---|---|
| $64^3$ | 38 | 0.049 | 0.91 | 20.8 | 12.6 | −0.36 | 0.75 |
| $64^3$ | 38 | 0.073 | 0.91 | 20.8 | 12.6 | −0.36 | 0.74 |
| $64^3$ | 38 | 0.098 | 0.91 | 20.8 | 12.6 | −0.37 | 0.74 |
| $64^3$ | 38 | 0.15 | 0.91 | 20.8 | 12.6 | −0.37 | 0.74 |
| $64^3$ | 38 | 0.20 | 0.91 | 20.8 | 12.6 | −0.35 | 0.74 |
| $64^3$ | 39 | 0.26 | 0.92 | 20.7 | 12.7 | −0.35 | 0.73 |
| $64^3$ | 39 | 0.34 | 0.92 | 20.7 | 12.7 | −0.34 | 0.73 |
| $64^3$ | 39 | 0.43 | 0.92 | 20.7 | 12.6 | −0.34 | 0.73 |
| $64^3$ | 39 | 0.52 | 0.92 | 20.7 | 12.7 | −0.31 | 0.72 |
| $64^3$ | 39 | 0.69 | 0.92 | 20.6 | 12.4 | −0.35 | 0.72 |
| $64^3$ | 37 | 0.88 | 0.91 | 20.7 | 11.8 | −0.57 | 0.74 |
| $128^3$ | 78 | 0.055 | 0.72 | 45.1 | 17.5 | −0.45 | 0.52 |
| $128^3$ | 79 | 0.081 | 0.72 | 45.0 | 17.7 | −0.45 | 0.51 |
| $128^3$ | 77 | 0.11 | 0.71 | 45.2 | 17.5 | −0.46 | 0.52 |
| $128^3$ | 78 | 0.16 | 0.71 | 45.2 | 17.5 | −0.44 | 0.52 |
| $128^3$ | 78 | 0.22 | 0.72 | 45.1 | 17.5 | −0.45 | 0.52 |
| $128^3$ | 78 | 0.29 | 0.72 | 45.1 | 17.6 | −0.44 | 0.51 |
| $128^3$ | 79 | 0.38 | 0.72 | 45.1 | 17.7 | −0.43 | 0.51 |
| $128^3$ | 79 | 0.48 | 0.73 | 44.8 | 17.6 | −0.42 | 0.50 |
| $128^3$ | 81 | 0.58 | 0.73 | 44.7 | 17.7 | −0.41 | 0.49 |
| $128^3$ | 81 | 0.76 | 0.75 | 44.3 | 17.3 | −0.58 | 0.47 |
| $128^3$ | 81 | 0.96 | 0.76 | 44.1 | 16.7 | −1.12 | 0.46 |

TABLE II. Simulation parameters and resulting flow statistics for $256^3$ and $512^3$ grid resolutions.

| Resolution | $\mathrm{Re}_\lambda$ | $M_t$ | $\eta/\Delta x$ | $L_I/\eta$ | $\lambda/\eta$ | $S_3$ | $D=\epsilon L_I/(u'/\sqrt{3})^3$ |
|---|---|---|---|---|---|---|---|
| $256^3$ | 111 | 0.057 | 0.83 | 73.2 | 20.8 | −0.48 | 0.49 |
| $256^3$ | 110 | 0.086 | 0.82 | 73.2 | 20.8 | −0.48 | 0.49 |
| $256^3$ | 111 | 0.11 | 0.83 | 73.1 | 20.8 | −0.49 | 0.49 |
| $256^3$ | 111 | 0.17 | 0.83 | 73.1 | 20.8 | −0.49 | 0.49 |
| $256^3$ | 110 | 0.23 | 0.81 | 73.2 | 20.7 | −0.49 | 0.49 |
| $256^3$ | 112 | 0.30 | 0.83 | 72.9 | 21.0 | −0.48 | 0.48 |
| $256^3$ | 112 | 0.40 | 0.83 | 72.9 | 20.9 | −0.47 | 0.48 |
| $256^3$ | 113 | 0.50 | 0.83 | 72.8 | 20.9 | −0.46 | 0.47 |
| $256^3$ | 115 | 0.61 | 0.84 | 72.3 | 21.0 | −0.46 | 0.46 |
| $256^3$ | 114 | 0.81 | 0.85 | 71.5 | 20.3 | −0.80 | 0.45 |
| $256^3$ | 114 | 1.01 | 0.87 | 71.3 | 19.5 | −1.54 | 0.43 |
| $512^3$ | 172 | 0.057 | 0.83 | 141 | 25.9 | −0.53 | 0.46 |
| $512^3$ | 176 | 0.086 | 0.82 | 145 | 26.2 | −0.54 | 0.45 |
| $512^3$ | 174 | 0.11 | 0.87 | 135 | 25.9 | −0.52 | 0.44 |
| $512^3$ | 174 | 0.17 | 0.87 | 136 | 25.8 | −0.52 | 0.46 |
| $512^3$ | 176 | 0.23 | 0.86 | 137 | 26.0 | −0.52 | 0.46 |
| $512^3$ | 178 | 0.30 | 0.83 | 141 | 26.3 | −0.52 | 0.46 |
| $512^3$ | 178 | 0.40 | 0.84 | 140 | 26.2 | −0.51 | 0.45 |
| $512^3$ | 176 | 0.50 | 0.86 | 136 | 25.9 | −0.50 | 0.44 |
| $512^3$ | 177 | 0.60 | 0.86 | 136 | 25.9 | −0.50 | 0.44 |
| $512^3$ | 176 | 0.81 | 0.88 | 134 | 25.2 | −0.82 | 0.43 |
| $512^3$ | 176 | 1.01 | 0.90 | 133 | 24.3 | −1.69 | 0.41 |

TABLE III. Simulation parameters and resulting flow statistics for $1024^3$ grid resolution.

| Resolution | $\mathrm{Re}_\lambda$ | $M_t$ | $\eta/\Delta x$ | $L_I/\eta$ | $\lambda/\eta$ | $S_3$ | $D=\epsilon L_I/(u'/\sqrt{3})^3$ |
|---|---|---|---|---|---|---|---|
| $1024^3$ | 350 | 0.11 | 0.64 | 371 | 36.5 | −0.55 | 0.41 |
| $1024^3$ | 355 | 0.17 | 0.64 | 374 | 36.8 | −0.55 | 0.43 |
| $1024^3$ | 369 | 0.23 | 0.62 | 382 | 37.7 | −0.56 | 0.41 |
| $1024^3$ | 361 | 0.30 | 0.58 | 395 | 37.4 | −0.55 | 0.44 |
| $1024^3$ | 365 | 0.40 | 0.59 | 390 | 37.6 | −0.54 | 0.43 |
| $1024^3$ | 253 | 0.51 | 1.00 | 233 | 31.2 | −0.53 | 0.44 |
| $1024^3$ | 262 | 0.60 | 1.02 | 231 | 31.6 | −0.53 | 0.42 |
| $1024^3$ | 261 | 0.79 | 1.05 | 229 | 30.9 | −0.83 | 0.41 |
| $1024^3$ | 250 | 1.02 | 1.04 | 226 | 29.1 | −1.95 | 0.42 |

in each direction. Consequently, the resolution parameter $k_{\max}\eta$ is in the range $1.82 < k_{\max}\eta < 3.30$, where the largest wave number $k_{\max}$ is half of the number of grids $N$ in each direction: $k_{\max} = N/2 = \pi/\Delta x$. For a high turbulent Mach number $M_t \geqslant 0.5$, the resolution parameter $\eta/\Delta x > 0.7$ and $k_{\max}\eta > 2.2$ in our numerical simulations. It was found that the resolutions of $\eta/\Delta x \geqslant 0.5$ are sufficient for the convergence of high-order moments of velocity gradients, for $M_t \leqslant 0.6$ [9]. We note that the highest turbulent Mach number is about 1.0 in our numerical simulations. Most shocklets are weak and have finite thickness at the scales typically comparable to the Kolmogorov length scale for $M_t \approx 1.0$ [14]. In order to resolve most of the shocklets, we choose higher resolution parameters $k_{\max}\eta > 2.2$ in compressible turbulence as compared to $k_{\max}\eta \approx 1$ in incompressible isotropic turbulence [14]. Previous studies showed that convergent small-scale statistics can be obtained at resolutions $k_{\max}\eta \approx 2.0$ at the turbulent Mach number $M_t = 1.0$ [13,14]. Therefore, the overall statistics should be well converged in our numerical simulations.

The integral length scale $L_I$ is defined by

$$L_I = \frac{3\pi}{2(u')^2}\int_0^\infty \frac{E(k)}{k}dk, \tag{40}$$

where $E(k)$ is the spectrum of kinetic energy per unit mass, namely, $\int_0^\infty E(k)dk = (u')^2/2$. We also calculate the velocity derivative skewness $S_3$, which is defined by

$$S_3 = \frac{[\langle(\partial u_1/\partial x_1)^3 + (\partial u_2/\partial x_2)^3 + (\partial u_3/\partial x_3)^3\rangle]/3}{\{\langle(\partial u_1/\partial x_1)^2 + (\partial u_2/\partial x_2)^2 + (\partial u_3/\partial x_3)^2\rangle/3\}^{3/2}}. \tag{41}$$

We present that for relatively small turbulent Mach numbers $M_t \leqslant 0.6$, values of $S_3$ are similar to typical values of $-0.6$ to $-0.4$ in incompressible turbulence [39]. At higher turbulent Mach numbers $M_t \geqslant 0.8$, the magnitude of $S_3$ becomes larger, due to the formation of shocklets in compressible turbulence [13]. We also calculate the normalized dissipation rate: $D = \epsilon L_I/(u'/\sqrt{3})^3$. The factor $\sqrt{3}$ is due to the fact that $u'$ is the root mean square value of the velocity magnitude in our study, which is different from the definition of the root mean square value of the velocity component in incompressible turbulence. We find that the normalized dissipation $D$ decreases with the increase of Taylor Reynolds number and approaches an asymptotic value at high Taylor Reynolds numbers. The typical values of $D$ are in the range of $0.4 < D < 0.5$ at Taylor Reynolds numbers $\mathrm{Re}_\lambda \geqslant 110$. These observations are consistent with previous studies in incompressible turbulence [40,41] and compressible turbulence [9].

## V. NUMERICAL RESULTS ON SPECTRA

### A. Transition between the pseudosound mode and the acoustic mode

Now we begin to study the transition between the pseudosound mode and the acoustic mode by numerical simulations. We plot $E^{cc}(k)/E^c(k)$ as a function of the normalized wave number $k\eta$

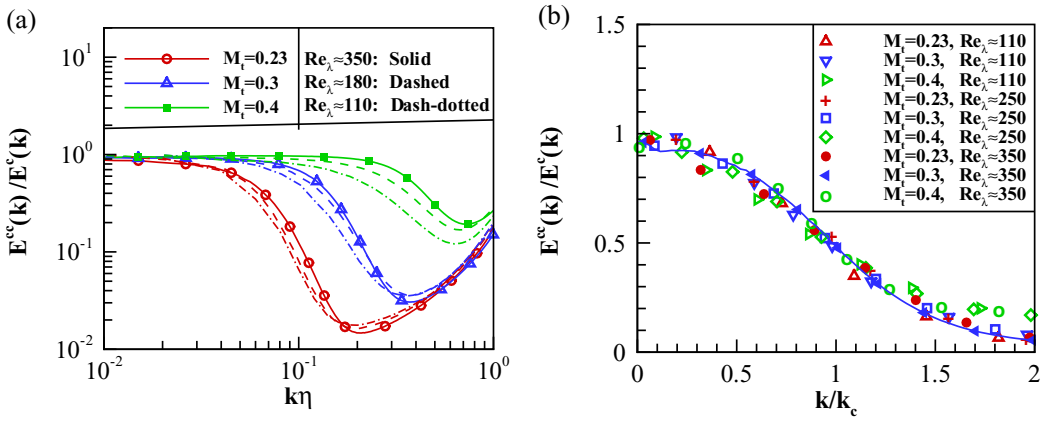


FIG. 1. The ratio of $E^{cc}(k)$ to $E^c(k)$ as a function of (a) $k\eta$, and (b) $k/k_c$.

at three different turbulent Mach numbers $M_t = 0.23$, 0.30, and 0.40 and at three different Taylor Reynolds numbers $\mathrm{Re}_\lambda \approx 110$, 180, and 350 in Fig. 1(a). The curves for three Taylor Reynolds numbers almost overlap at each turbulent Mach number $M_t$, indicating that $E^{cc}(k)/E^c(k)$ is nearly a universal function of the normalized wave number $k\eta$ at turbulent Mach number $M_t \leqslant 0.4$, for the case of purely solenoidal forcing. As $M_t$ becomes smaller, the acoustic-mode-dominated wave-number range becomes narrower. It is easier for acoustic waves to be generated at a larger turbulent Mach number and at a smaller wave number. In particular, the acoustic mode always dominates at $k\eta = 0.01$ for the three turbulent Mach numbers.

We define the critical wave number at small turbulent Mach numbers $M_t \leqslant 0.4$ as follows:

$$E^c(k_c; M_t) = 2E^{cs}(k_c; M_t), \tag{42}$$

where the spectrum $E^c(k)$ of the compressible velocity $\boldsymbol{u}^c$ is twice the spectrum $E^{cs}(k)$ of the pseudosound velocity $\boldsymbol{u}^{cs}$ at the critical wave number $k_c$. Generally, for $k < k_c$, the acoustic mode dominates over the pseudosound mode: $E^{cc}(k) > E^{cs}(k)$. For $k > k_c$, the pseudosound mode dominates over the acoustic mode: $E^{cs}(k) > E^{cc}(k)$. Similarly, at a given wave number $k$, we can find a critical turbulent Mach number $M_{tc}(k)$ where the compressible velocity field satisfies following condition:

$$E^c(k; M_{tc}) = 2E^{cs}(k; M_{tc}). \tag{43}$$

The acoustic mode dominates over the pseudosound mode at larger turbulent Mach numbers $M_t > M_{tc}$, while the pseudosound mode dominates over the acoustic mode at smaller turbulent Mach numbers $M_t < M_{tc}$.

We plot $E^{cc}(k)/E^c(k)$ as a function of $k/k_c$ in Fig. 1(b). We then show that values of $E^{cc}(k)/E^c(k)$ are well rescaled in terms of $k_c$ near the transitional point $k \sim k_c$: All values of $E^{cc}(k)/E^c(k)$ almost overlap for the wave number $k$ close to the critical wave number $k_c$. Moreover, the acoustic mode dominates at small wave numbers, $E^{cc}(k)/E^c(k) \approx 1$ as wave number $k$ decreases from $k_c$, and becomes negligible at large wave numbers, $E^{cc}(k)/E^c(k) \approx 0$ as wave number $k$ increases from $k_c$. To sum up, we have demonstrated that in the case of purely solenoidal forcing, the transition between the pseudosound mode and the acoustic mode in the inertial range is quite universal for different Taylor Reynolds numbers $\mathrm{Re}_\lambda$ and different turbulent Mach numbers $M_t$: (1) For a fixed small turbulent Mach number $M_t \leqslant 0.4$, the normalized spectrum $E^{cc}(k)/E^c(k)$ depends only on the normalized wave number $k\eta$ and (2) near the transitional point $k/k_c \sim 1$, the behavior of the normalized spectrum $E^{cc}(k)/E^c(k)$ can be described by a universal function of $k/k_c$ that is not affected by $M_t$.

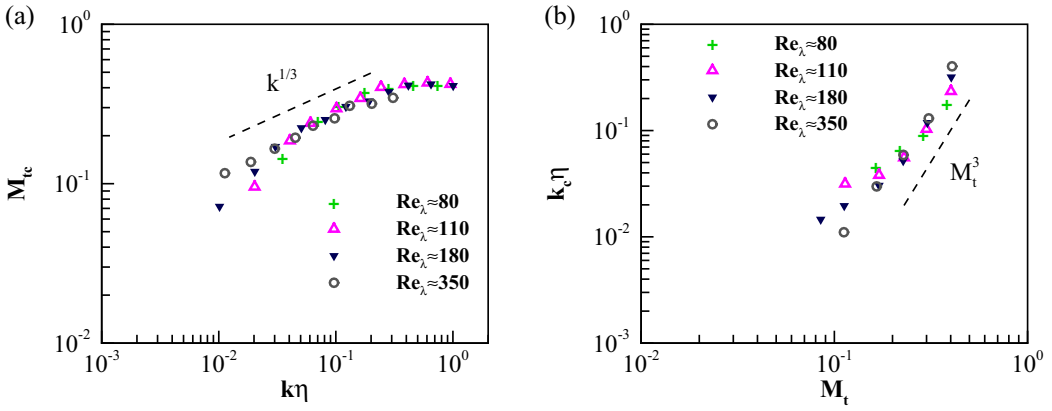


FIG. 2. (a) The critical turbulent Mach number as a function of the normalized wave number. (b) The normalized critical wave number as a function of the turbulent Mach number.

In Fig. 2(a), we plot the critical turbulent Mach number $M_{tc}$ as a function of the normalized wave number $k\eta$. The critical turbulent Mach number is calculated from the simulated flows by linear interpolation. Specifically, we estimate $M_{tc}$ as $M_{tc} = (r_1 M_{t2} + r_2 M_{t1})/(r_1 + r_2)$, where $M_{t1} < M_{t2}$, $r_1 = 2 - E^c(k; M_{t1})/E^{cs}(k; M_{t1}) > 0$, and $r_2 = E^c(k; M_{t2})/E^{cs}(k; M_{t2}) - 2 > 0$. For example, the critical Mach number $M_{tc}$ in the range of $0.11 < M_{tc} < 0.17$ is obtained from the simulated flows at $M_{t1} = 0.11$ and $M_{t2} = 0.17$ by using linear interpolation. In Fig. 2(a), we show that the $M_{tc}$ curves at different Taylor Reynolds numbers almost collapse into a single universal function of $k\eta$: (1) For the dissipation range of $k\eta \geqslant 0.3$, the critical turbulent Mach number is close to a constant 0.4, $M_{tc} \approx 0.4$, and (2) for the inertial range of $k\eta \leqslant 0.3$, the critical turbulent Mach number decreases with the decrease of wave number. We also observe a scaling behavior: $M_{tc} \sim k^{1/3}$ in a short range of wave number $0.02 \leqslant k\eta \leqslant 0.2$. We find that the acoustic mode becomes dominant for $M_t \geqslant M_{tc}$. Particularly, we pointed out that in the developed acoustic region $M_t \geqslant 0.4$, the acoustic mode dominates in both the inertial range and dissipation range. The viscosity effect becomes important at $M_t \leqslant 0.4$, where the pseudosound mode dominates in the dissipation range. In the inertial range, $M_{tc}$ decreases with the decrease of $k\eta$, implying that it is easier to generate the acoustic mode at larger scales.

In Fig. 2(b), we show the normalized critical wave number $k_c\eta$ as a function of turbulent Mach number at different Taylor Reynolds numbers. We observe a scaling relation $k_c \sim M_t^3$ in a short range of turbulent Mach number $0.17 \leqslant M_t \leqslant 0.4$. We show that at a given turbulent Mach number $M_t \leqslant 0.4$, the entire spectrum of the compressible velocity can be divided into two distinct parts: (1) the acoustic mode dominates at large scales $k \leqslant k_c$ and (2) the pseudosound mode dominates at small scales $k \geqslant k_c$. As the turbulent Mach number becomes smaller, the wave-number range of the pseudosound mode increases quickly. Thus, for fully developed compressible turbulence, at a given Reynolds number, the pseudosound mode will eventually dominate over the entire wave-number range as $M_t$ decreases, giving rise to the following spectrum scaling for the compressible velocity, $E^c(k) \sim M_t^4 k^{-3}$, as shown in Eq. (38). It is worth noting that to understand the transition between the pseudosound mode and the acoustic mode in the case of purely solenoidal forcing, we only need to study the weakly compressible turbulence at $M_t \leqslant 0.4$. For higher turbulent Mach numbers $M_t \geqslant 0.5$, the pseudosound mode no longer dominates at any scale.

We plot some instantaneous snapshots of velocity divergence in a subdomain with $384^3$ grids, for the simulations with $1024^3$ grid resolution at different turbulent Mach numbers $M_t = 0.23$, 0.3, 0.4, 0.6, 0.8, and 1.0 in Fig. 3. We observe that as the turbulent Mach increases from $M_t = 0.23$, the isosurfaces of $\theta = -2\theta'$ become slightly flatter at $M_t = 0.4$, indicating that some localized shocklets are generated at $M_t = 0.4$ [3]. The length scales of shocklets are quite small at $M_t = 0.4$ [3]. We also show that as the turbulent Mach number increases from $M_t = 0.4$,

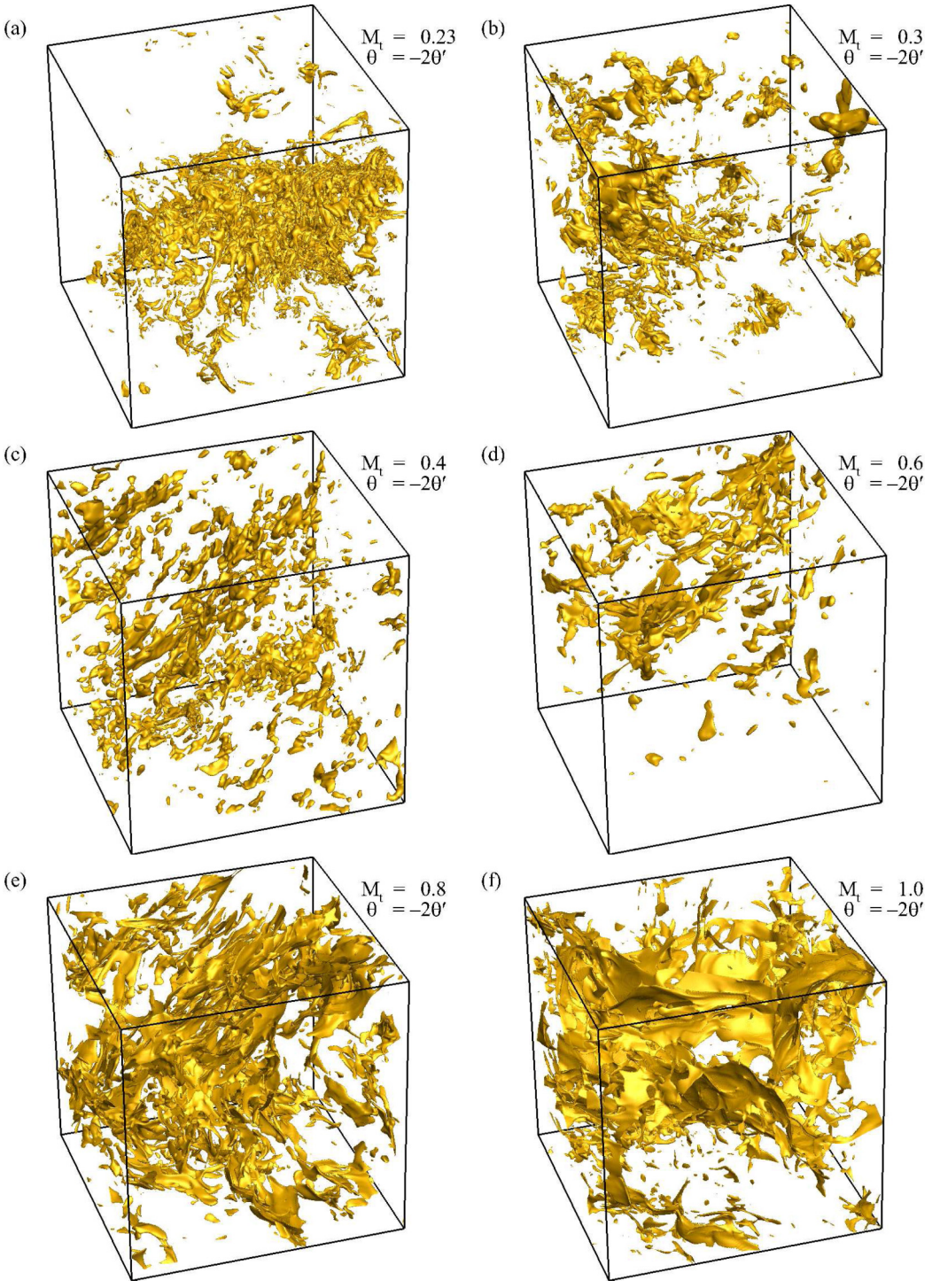


FIG. 3. Isosurfaces of velocity divergence in a subdomain with $384^3$ grids, for the simulations with $1024^3$ grid resolution at different turbulent Mach numbers $M_t = 0.23$, 0.3, 0.4, 0.6, 0.8, and 1.0 for $\mathrm{Re}_\lambda \approx 350$ and 250.

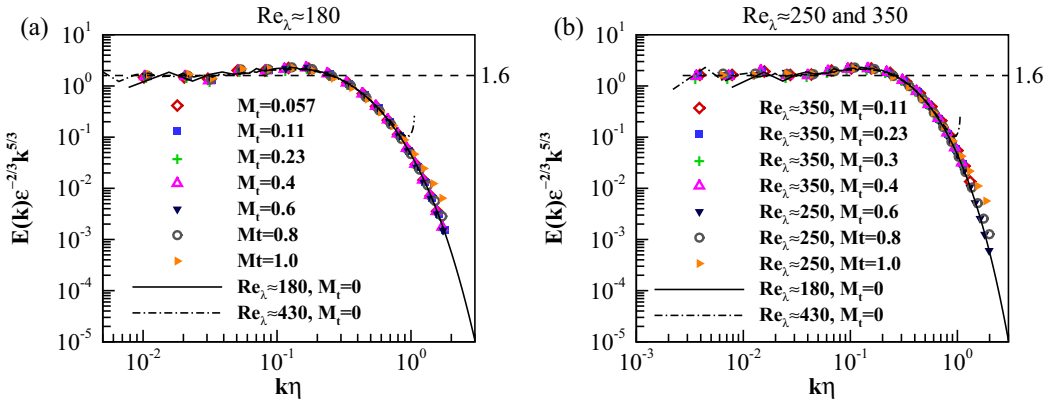


FIG. 4. Compensated spectrum of velocity at $\mathrm{Re}_\lambda \approx 180$, 250, and 350. The solid line and dash-dotted line represent the compensated spectrum of velocity in incompressible isotropic turbulence at $\mathrm{Re}_\lambda \approx 180$ and 430 respectively [38,42].

the thickness of the isosurface becomes smaller, and the transverse length scale becomes larger at $M_t = 0.8$, implying that the shocklets become stronger.

### B. Spectra of velocity and its compressible component

In Fig. 4, we plot the compensated spectrum of velocity $E(k)\epsilon^{-2/3}k^{5/3}$ at different turbulent Mach numbers and at $\mathrm{Re}_\lambda \approx 180$, 250, and 350. We can identify an inertial range with a Kolmogorov constant of approximately 1.6, similar to the velocity spectrum of incompressible turbulence. The compensated spectrum curves overlap in all scales for $M_t \leqslant 0.8$. At $M_t = 1.0$, the compensated spectrum of velocity is slightly larger at small scales $k\eta > 1.0$, owing to the effect of the compressibility. In addition, we plot the velocity spectrum of incompressible turbulence at $\mathrm{Re}_\lambda \approx 180$ and 430 [38,42]. We show that the solid and dashed-dotted lines overlap at high $k$. We also find that the velocity spectrum of compressible turbulence at turbulent Mach numbers $M_t \leqslant 0.8$ almost overlap with the velocity spectrum of incompressible turbulence. The observations of the velocity spectrum are consistent with previous studies [13,14,24].

According to previous analysis, for weakly compressible turbulence, the statistics of the compressible velocity component can be well described by the pseudosound constitutive relationship at relatively small scales, where the inertial spectrum $E^c(k)$ is given by Eq. (36). We plot the compensated spectrum $E^c(k)M_t^{-4}L_I^{4/3}\epsilon^{-2/3}k^3$ of the compressible velocity at $\mathrm{Re}_\lambda \approx 180$ and 350 in Figs. 5(a) and 6(a). The solid line and dash-dotted line represent the compensated spectrum $E^{cs}(k)M_t^{-4}L_I^{4/3}\epsilon^{-2/3}k^3$ for the pseudosound velocity $\boldsymbol{u}^{cs}$. We do not observe a clear and definite plateau of the compensated spectrum $E^{cs}(k)M_t^{-4}L_I^{4/3}\epsilon^{-2/3}k^3$ at $\mathrm{Re}_\lambda \approx 180$. At $\mathrm{Re}_\lambda \approx 350$, we can see a very narrow plateau: $E^{cs}(k)M_t^{-4}L_I^{4/3}\epsilon^{-2/3}k^3 \approx C_v^{PS}$ in the range of $0.015 \leqslant k\eta \leqslant 0.03$, where the constant $C_v^{PS} \approx 0.55$. A similar observation has been reported for the pressure spectrum of incompressible turbulence [43,44]. A misleading $k^{-5/3}$ scaling of the pressure spectrum can be observed for low and moderate Taylor Reynolds numbers, mainly due to the spectral bump at the end of the inertial range. The appearance of a $k^{-7/3}$ scaling is apparent only at $\mathrm{Re}_\lambda \geqslant 400$ as shown by Gotoh and Fukayama [43] and Tsuji and Ishihara [44]. Since the pseudosound velocity component is closely related to the solenoidal pressure, it is reasonable that we cannot observe a wide scaling range at $\mathrm{Re}_\lambda \leqslant 350$.

We plot the compensated spectrum of the compressible velocity component at $M_t = 0.11$ and $\mathrm{Re}_\lambda \approx 110$, 250, and 350 in Fig. 7. We find that the compensated spectrum does not overlap at small scales for different Taylor Reynolds numbers. This is due to the low Reynolds number effect. We expect that the compensated spectrum will overlap at small scales for large enough

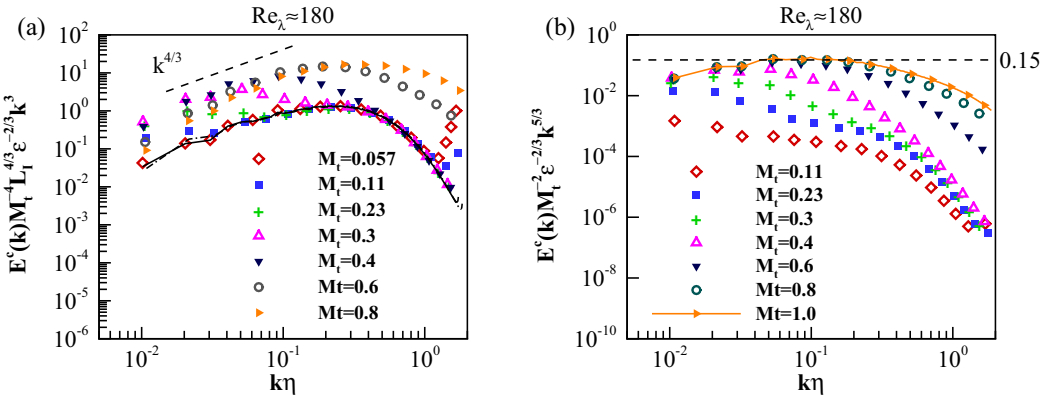


FIG. 5. Compensated spectrum of the compressible velocity at $\mathrm{Re}_\lambda \approx 180$. (a) $E^c(k)M_t^{-4}L_I^{4/3}\epsilon^{-2/3}k^3$. The solid line and dash-dotted line represent the compensated spectrum of the pseudosound velocity $E^{cs}(k)M_t^{-4}L_I^{4/3}\epsilon^{-2/3}k^3$ at $M_t = 0.057$ and 0.11 respectively. (b) $E^c(k)M_t^{-2}\epsilon^{-2/3}k^{5/3}$.

Taylor Reynolds numbers. The behavior of the compensated spectrum of the compressible velocity component at small scales is similar to the behavior of the compensated spectrum of the pressure in incompressible turbulence [43]. The compensated spectrum of the pressure overlap at small scales only for $\mathrm{Re}_\lambda > 400$ in incompressible turbulence. Gotoh and Fukayama [43] reported a small plateau between $0.007 \leqslant k\eta \leqslant 0.04$ for the compensated pressure spectrum at $\mathrm{Re}_\lambda > 300$. Here, we report a $k^{-5/3}$ scaling of velocity spectrum, and a $k^{-3}$ scaling of the spectrum of the compressible velocity component in the range of $0.007 \leqslant k\eta \leqslant 0.04$ at $M_t = 0.11$ and $\mathrm{Re}_\lambda \approx 350$. The compensated spectrum of the pseudo-sound velocity component at $M_t = 0.11$ and $\mathrm{Re}_\lambda \approx 110$, 250, and 350 is also plotted in Fig. 7, which exhibits a very narrow plateau between $0.015 \leqslant k\eta \leqslant 0.03$ at $M_t = 0.11$ and $\mathrm{Re}_\lambda \approx 350$.

From Figs. 5(a) and 6(a), we observe that the compensated spectrum of the compressible velocity has an overlapped region with the compensated spectrum of the pseudosound velocity, at low turbulent Mach numbers and at high wave numbers. In particular, the two spectra overlap only for a narrow range $k\eta \geqslant 0.4$ at $M_t = 0.4$. As the turbulent Mach number decreases, the overlapping region of the two spectra gradually extends into the inertial range. For the turbulent Mach number of 0.057, the compressible velocity spectrum satisfies the pseudosound constitutive relationship

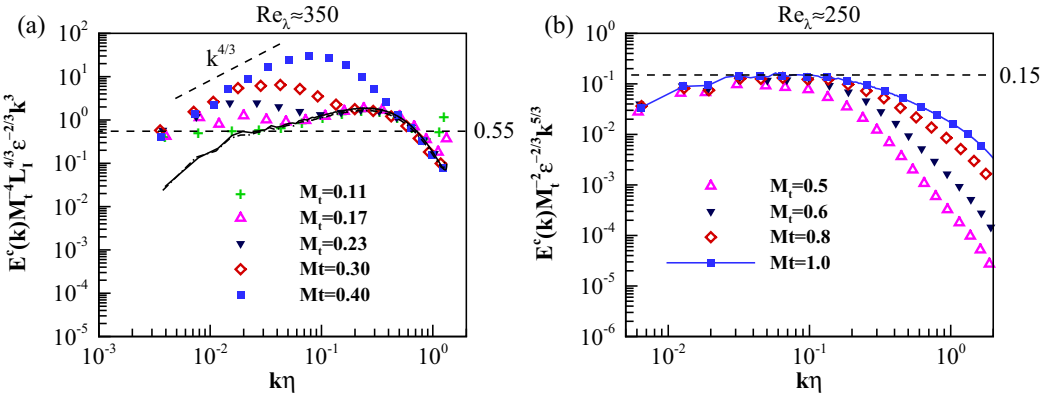


FIG. 6. Compensated spectrum of the compressible velocity at $\mathrm{Re}_\lambda \approx 250$ and 350. (a) $E^c(k)M_t^{-4}L_I^{4/3}\epsilon^{-2/3}k^3$. The solid line and dash-dotted line represent the compensated spectrum of the pseudosound velocity $E^{cs}(k)M_t^{-4}L_I^{4/3}\epsilon^{-2/3}k^3$ at $M_t = 0.11$ and 0.23 respectively. (b) $E^c(k)M_t^{-2}\epsilon^{-2/3}k^{5/3}$.

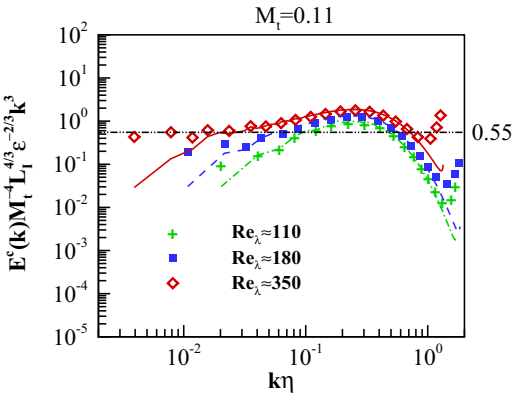


FIG. 7. Compensated spectrum of the compressible velocity at $M_t = 0.11$ and $\mathrm{Re}_\lambda \approx 110$, 250, and 350. The dash-dotted line, dashed line, and solid line represent the compensated spectrum of the pseudosound velocity: $E^{cs}(k)M_t^{-4}L_I^{4/3}\epsilon^{-2/3}k^3$ at $\mathrm{Re}_\lambda \approx 110$, 250, and 350 respectively.

$E^c(k) = E^{cs}(k)$ over the entire range of wave numbers. Thus, for any given Taylor Reynolds number, we infer that as turbulent Mach number becomes much smaller, the pseudosound mode will dominate over acoustic mode at all scales. It is important to note that if the Taylor Reynolds number is large enough, there will be a $M_t^4k^{-3}$ scaling for the spectrum $E^c(k)$ of the compressible velocity when turbulent Mach number is very small. The same $M_t^4k^{-3}$ scaling for the spectrum $E^c(k)$ has been obtained by an EDQNM model [1,27].

Generally, for weakly compressible turbulence, the spectrum of the compressible velocity may not obey a single scaling in the inertial range. Considering an ideal situation of a large enough Taylor Reynolds number, we can identify a critical wave number $k_c$ for the transition between the pseudosound mode and acoustic mode. For $k \geqslant k_c$ in the inertial range, we already showed that $E^c(k) \sim M_t^4k^{-3}$ according to the pseudosound relationship and the classical Kolmogorov turbulence theory. Until now, little knowledge has been obtained on the behavior of $E^c(k)$ at $k \leqslant k_c$ in the inertial range. The mixed scaling relations in the inertial range of the compressible velocity spectrum have also been revealed by an EDQNM model [1,27]. The analysis on the EDQNM model provided three different spectral zones: an acoustic region, a transition region, and a pseudosound region.

For the fully developed acoustic region at high turbulent Mach numbers, we assume that the ratio of the compressible velocity to the solenoidal velocity fluctuations is proportional to the turbulent Mach number $M_t$ [29]. We also assume that the inertial scaling behavior of the spectrum of the compressible velocity is similar to the spectrum of the solenoidal velocity. Based on these assumptions, we show that the spectrum of the compressible velocity satisfies $E^c(k) \sim M_t^2\epsilon^{2/3}k^{-5/3}$ at high turbulent Mach numbers. We plot the compensated spectrum $E^c(k)M_t^{-2}\epsilon^{-2/3}k^{5/3}$ at different turbulent Mach numbers in Figs. 5(b) and 6(b). We observe that there is an excellent collapse of $E^c(k)M_t^{-2}\epsilon^{-2/3}k^{5/3}$ at small wave numbers for different turbulent Mach numbers $M_t \geqslant 0.3$, which demonstrates that the acoustic mode amplitude gives rise to a $M_t$ scaling of the compressible velocity. We also show a narrow plateau of the spectrum for large turbulent Mach numbers $M_t \geqslant 0.5$: $E^c(k)M_t^{-2}\epsilon^{-2/3}k^{5/3} \approx 0.15$. A similar narrow plateau of the spectrum of the compressible velocity was observed in previous works for $M_t$ of approximately 1.0 [13,14]. In a previous DNS study, Donzis and Jagannathan [24] plotted the normalized energy spectrum $E^c(k)\epsilon^{-2/3}k^{5/3}$ of the compressible velocity at $M_t = 0.1$, 0.3, 0.6. They did not give any definite scaling exponent of the compressible spectrum $E^c(k)$ in the inertial range. Their figure showed a narrow plateau of the normalized spectrum of the compressible velocity at $M_t = 0.6$. Our numerical result is similar at $M_t = 0.6$. It is not easy to observe a clear scaling behavior of $E^c(k)$ at $M_t = 0.3$ from numerical simulations, even for the situation of large scale direct numerical simulation using the grid resolution of $2048^3$ performed by Donzis and Jagannathan [24].

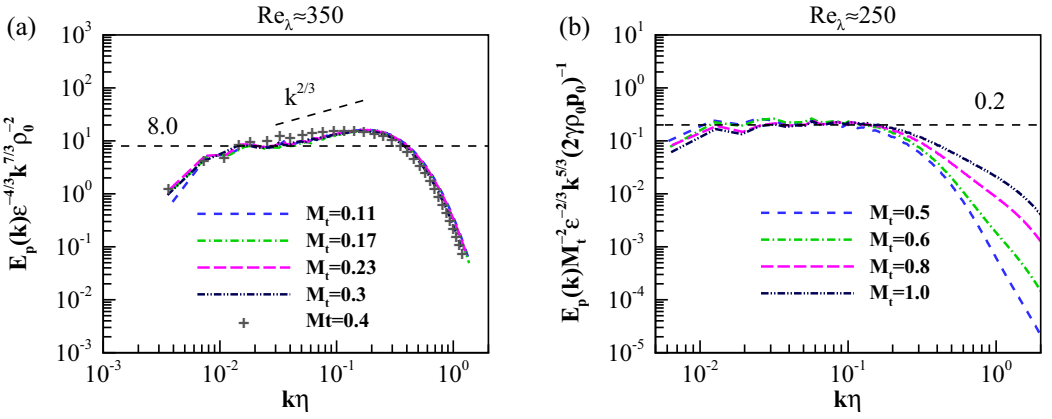


FIG. 8. Compensated spectrum of pressure at different turbulent Mach numbers for $\mathrm{Re}_\lambda \approx 350$ and 250.

### C. Spectra of pressure, density, and temperature

We consider the spectrum of pressure $E_p(k)$ at different Mach numbers in compressible turbulence, where the pressure spectrum obeys the relation $\int_0^\infty E_p(k)dk = \langle (p-p_0)^2 \rangle$. A previous study revealed that at low turbulent Mach numbers $M_t < 0.3$, the fluctuation of the compressible pressure component is much smaller than its solenoidal counterpart, while at high turbulent Mach numbers $M_t > 0.3$, the fluctuation of the compressible pressure component has the same order of the magnitude as the solenoidal component [9]. Thus, we need to normalize the pressure spectrum in different manners for different turbulent Mach numbers.

For the case of a low turbulent Mach number, we consider the following normalization of the pressure spectrum: $E_p(k)\epsilon^{-4/3}k^{7/3}\rho_0^{-2}$, which is the same as the case of incompressible turbulence [43]. In incompressible turbulence, the density is constant and does not appear in the normalization. We plot the compensated spectrum of pressure at $\mathrm{Re}_\lambda \approx 350$ and at turbulent Mach number ranging from 0.11 to 0.4 in Fig. 8(a). At $M_t \leqslant 0.3$, the compensated pressure spectrum overlaps with one another and exhibits a small plateau between $0.015 \leqslant k\eta \leqslant 0.04$: $E_p(k)\epsilon^{-4/3}k^{7/3}\rho_0^{-2} \approx 8.0$. We also observe a bump with the slope close to 2/3 in the range of $0.04 \leqslant k\eta \leqslant 0.2$, indicating that the pressure spectrum exhibit a $k^{-5/3}$ scaling at the end of the inertial range. The observations are consistent with the case of incompressible turbulence [43]. A previous DNS study showed a scaling of $E_p(k) \sim k^{-5/3}$ at relatively low Taylor Reynolds numbers in weakly compressible isotropic turbulence [24].

From Fig. 8(a), we observe that at $M_t = 0.4$, the compensated pressure spectrum is larger than those at low turbulent Mach numbers and does not exhibit any plateau. We note that the compensated spectrum of the solenoidal pressure component at $M_t = 0.4$ is similar to that of the incompressible turbulence. The difference of the compensated pressure spectrum between $M_t = 0.4$ and $M_t \leqslant 0.3$ can be attributed to the effect of the compressible pressure component. As turbulence Mach number increases from $M_t = 0.4$, the impact of the compressible component on the pressure spectrum becomes larger. According to the equipartition relation between the compressible velocity and compressible pressure in the acoustic scenario [16], we assume that $E_p^c(k) \sim 2\rho_0^2 c_0^2 E^c(k)$, where $c_0$ is the average speed of sound, $E_p^c(k)$ is the spectrum of compressible pressure component, and $E^c(k)$ is the spectrum of compressible velocity component. The relation $E_p^c(k) \sim 2\rho_0^2 c_0^2 E^c(k)$ was verified at the turbulent Mach numbers $M_t = 0.3$ and 0.6 by Jagannathan and Donzis [9]. Moreover, we assume that the pressure spectrum $E_p(k)$ has the same scaling as the spectrum of the compressible pressure component $E_p^c(k)$ at high turbulent Mach numbers. Thus, we have the relation $E_p(k) \sim 2\rho_0^2 c_0^2 E^c(k)$. Provided the scaling of $E^c(k) \sim M_t^2 \epsilon^{2/3} k^{-5/3}$, we obtain $E_p(k) \sim 2\gamma\rho_0 p_0 M_t^2 \epsilon^{2/3} k^{-5/3}$ at high turbulent Mach numbers.

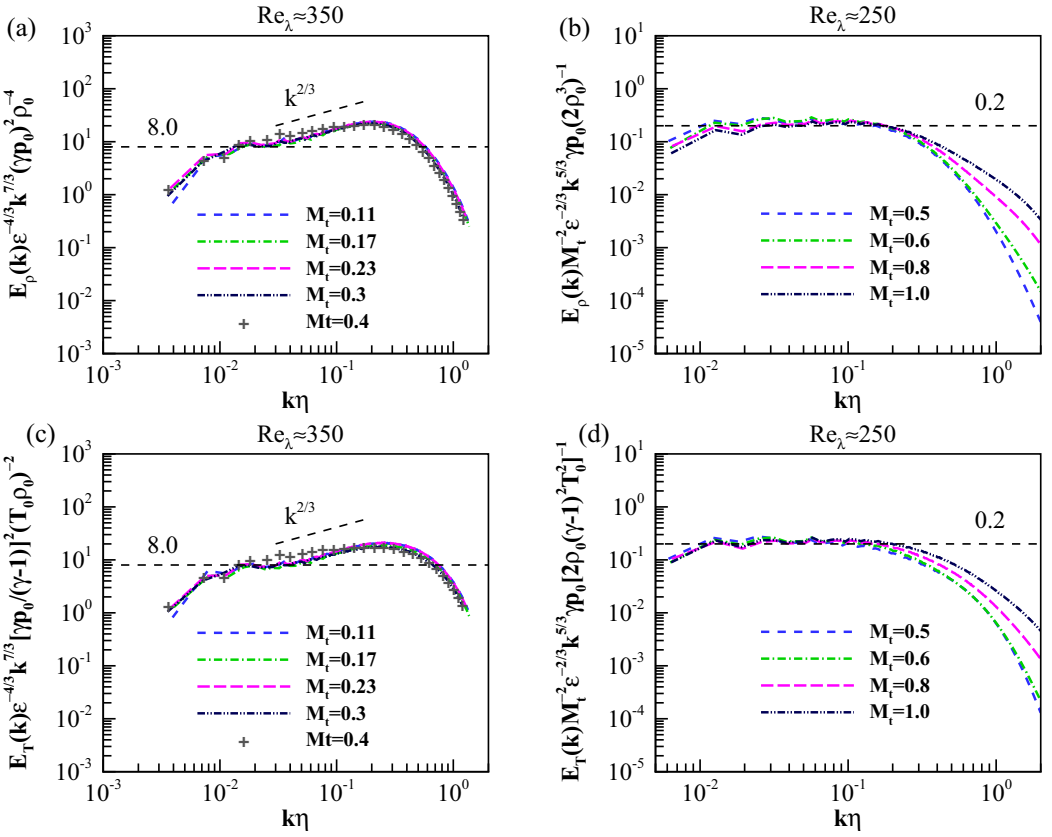


FIG. 9. Compensated spectra of density and temperature at different turbulent Mach numbers for $\mathrm{Re}_\lambda \approx 350$ and 250.

In Fig. 8(b), we depict the compensated spectrum of pressure $E_p(k)M_t^{-2}\epsilon^{-2/3}k^{5/3}(2\gamma\rho_0 p_0)^{-1}$ at $\mathrm{Re}_\lambda \approx 250$ and at a turbulent Mach number ranging from 0.5 up to 1.0. We observe a plateau between $0.02 \leqslant k\eta \leqslant 0.1$: $E_p(k)M_t^{-2}\epsilon^{-2/3}k^{5/3}(2\gamma\rho_0 p_0)^{-1} \approx 0.2$. The constant 0.2 is slightly larger than the constant 0.15 for the case of the compensated spectrum of the compressible velocity. At small scales $k\eta \geqslant 0.2$, the compensated spectrum of pressure increases with the increase in turbulent Mach number, which is similar to the behavior of the compensated spectrum of the compressible velocity. The $k^{-5/3}$ scaling of the pressure spectrum at high turbulent Mach numbers $M_t \geqslant 0.5$ is consistent with a previous study by Donzis and Jagannathan [24]. They reported the $k^{-5/3}$ scaling of the pressure spectrum at the turbulent Mach number $M_t = 0.6$.

We consider the spectra of density and temperature: $E_\rho(k)$ and $E_T(k)$, where $\int_0^\infty E_\rho(k)dk = \langle(\rho-\rho_0)^2\rangle$ and $\int_0^\infty E_T(k)dk = \langle(T-T_0)^2\rangle$. In previous analysis, we have assumed the isentropic relation $\gamma\rho'/\rho_0 = p'/p_0$ for the fluctuations of density and pressure: $\rho' = \rho - \rho_0$ and $p' = p - p_0$ at a low turbulent Mach number. Similarly, there is the isentropic relation $[\gamma/(\gamma-1)]T'/T_0 = p'/p_0$ for the fluctuations of temperature and pressure, where $T' = T - T_0$. We model the spectra of density and temperature based on the isentropic relations as $E_\rho(k) = E_p(k)\rho_0^2 p_0^{-2}\gamma^{-2}$ and $E_T(k) = E_p(k)T_0^2 p_0^{-2}[\gamma/(\gamma-1)]^{-2}$. Consequently, we have the following scaling relations: (1) $E_\rho(k) \sim (\gamma p_0)^{-2}\rho_0^4\epsilon^{4/3}k^{-7/3}$ and $E_T(k) \sim [\gamma p_0/(\gamma-1)]^{-2}(T_0\rho_0)^2\epsilon^{4/3}k^{-7/3}$ for low turbulent Mach numbers $M_t \leqslant 0.3$ and (2) $E_\rho(k) \sim 2\rho_0^3(\gamma p_0)^{-1}M_t^2\epsilon^{2/3}k^{-5/3}$ and $E_T(k) \sim 2(\gamma-1)^2\rho_0 T_0^2(\gamma p_0)^{-1}M_t^2\epsilon^{2/3}k^{-5/3}$ for high turbulent Mach numbers $M_t \geqslant 0.5$.

In Figs. 9(a) and 9(c), we plot the compensated spectra of density and temperature: $E_\rho(k)\epsilon^{-4/3}k^{7/3}(\gamma p_0)^2\rho_0^{-4}$ and $E_T(k)\epsilon^{-4/3}k^{7/3}[\gamma p_0/(\gamma-1)]^2(T_0\rho_0)^{-2}$ at $\mathrm{Re}_\lambda \approx 350$ and at a

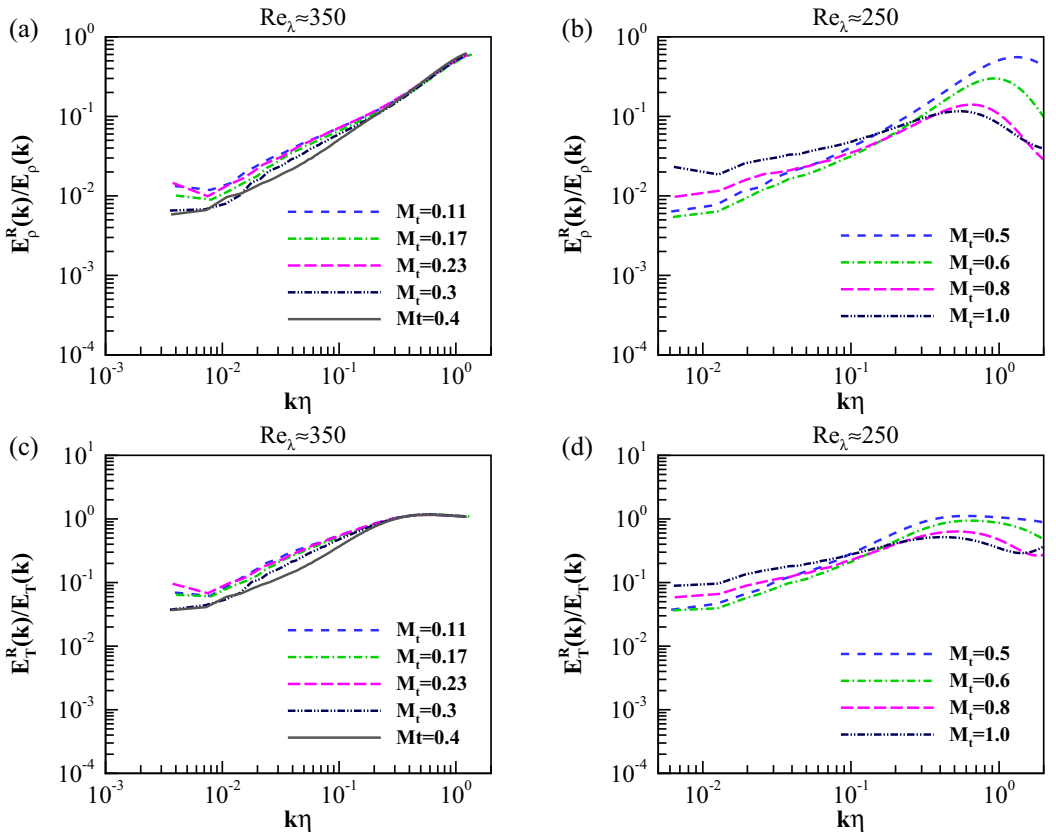


FIG. 10. Normalized spectra of the residual density and residual temperature at different turbulent Mach numbers for $\mathrm{Re}_\lambda \approx 350$ and 250.

turbulent Mach number ranging from 0.11 to 0.4. Similar to the compensated spectrum of pressure, we observe a small plateau for the compensated spectra of density and temperature: $E_\rho(k)\epsilon^{-4/3}k^{7/3}(\gamma p_0)^2\rho_0^{-4} \approx 8.0$ and $E_T(k)\epsilon^{-4/3}k^{7/3}[\gamma p_0/(\gamma-1)]^2(T_0\rho_0)^{-2} \approx 8.0$ in the range of $0.015 \leqslant k\eta \leqslant 0.04$, at a low turbulent Mach number $M_t \leqslant 0.3$. We observe a bump with a slope close to 2/3 in the range of $0.04 \leqslant k\eta \leqslant 0.2$ for the spectra of density and temperature. To sum up, we have clarified that at a low turbulent Mach number $M_t \leqslant 0.3$, the spectra of pressure, density, and temperature exhibit a $k^{-7/3}$ scaling in the inertial range in solenoidally forced compressible isotropic turbulence, similar to the spectrum of pressure in incompressible turbulence.

In Figs. 9(b) and 9(d), we plot the compensated spectra of density and temperature, $E_\rho(k)M_t^{-2}\epsilon^{-2/3}k^{5/3}\gamma p_0(2\rho_0^3)^{-1}$ and $E_T(k)M_t^{-2}\epsilon^{-2/3}k^{5/3}\gamma p_0[2\rho_0(\gamma-1)^2T_0^2]^{-1}$, at $\mathrm{Re}_\lambda \approx 250$ and at a turbulent Mach number ranging from 0.5 to 1.0. Similar to the compensated spectrum of pressure, we observe a plateau for the compensated spectra of density and temperature, $E_\rho(k)M_t^{-2}\epsilon^{-2/3}k^{5/3}\gamma p_0(2\rho_0^3)^{-1} \approx 0.2$ and $E_T(k)M_t^{-2}\epsilon^{-2/3}k^{5/3}\gamma p_0[2\rho_0(\gamma-1)^2T_0^2]^{-1} \approx 0.2$, in the range of $0.02 \leqslant k\eta \leqslant 0.1$ at high turbulent Mach numbers $M_t \geqslant 0.5$. At small scales $k\eta \geqslant 0.2$, the compensated spectra of density and temperature increase with the increase in turbulent Mach number. The $k^{-5/3}$ scaling of the spectra of density and temperature at high turbulent Mach numbers $M_t \geqslant 0.5$ is consistent with a previous study by Donzis and Jagannathan [24]. They reported the $k^{-5/3}$ scaling of the spectra of density and temperature at the turbulent Mach number $M_t = 0.6$.

To verify the isentropic relations among the fluctuations of pressure, density, and temperature, we define the residual density and residual temperature as $\rho^R = \rho' - \rho_0 p'/(\gamma p_0)$ and

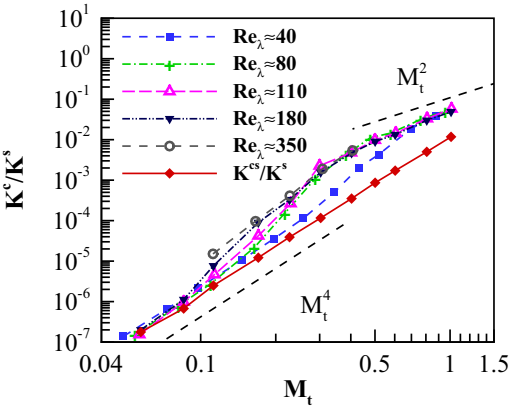


FIG. 11. Normalized energy of the compressible velocity component $K^c/K^s$. Normalized energy of the pseudosound velocity component $K^{cs}/K^s$ at $\mathrm{Re}_\lambda \approx 180$ is also plotted.

$T^R = T' - (\gamma - 1)T_0 p'/(\gamma p_0)$. We consider the normalized spectra of the residual density and residual temperature, $E_\rho^R(k)/E_\rho(k)$ and $E_\rho^R(k)/E_\rho(k)$, where $\int_0^\infty E_\rho^R(k)dk = \langle(\rho^R)^2\rangle$ and $\int_0^\infty E_T^R(k)dk = \langle(T^R)^2\rangle$. In Fig. 10, we plot the normalized spectra of the residual density and residual temperature at $\mathrm{Re}_\lambda \approx 350$ and 250 for different turbulent Mach numbers. We show that the normalized spectra of the residual density and residual temperature are much smaller than 1.0 in the range of $k\eta \leqslant 0.1$, indicating that the spectra of density and temperature exhibit the same inertial scaling as the spectrum of pressure in compressible turbulence. The normalized spectra of the residual density and residual temperature are close to 1.0 at small scales $k\eta \approx 1$, indicating that the isentropic relations are no longer valid at small scales $k\eta \approx 1$. The violation of the isentropic relations at small scales can be attributed to the effect of the thermal diffusion terms and viscous dissipation terms in the governing equations of pressure and temperature.

## VI. NUMERICAL RESULTS ON ONE POINT STATISTICS

### A. Mach number scaling of the energy and dissipation rate of the compressible velocity component

The previous arguments about the spectra help us to interpret the dependency of the various one-point statistics on the turbulent Mach number. In Fig. 11, we depict the ratio $K^c/K^s$ for different Taylor Reynolds numbers and different turbulent Mach numbers. At a fixed turbulent Mach number, the ratio is higher for a larger Taylor Reynolds number. A more interesting point is the effect of turbulent Mach number: There is no single scaling relation between the normalized energy of the compressible velocity component and turbulent Mach number. For a very small turbulent Mach number, typically $M_t < 0.1$, we observe that $K^c/K^s$ has a $M_t^4$ scaling. In the same figure, we also show the normalized energy $K^{cs}/K^s$ for the pseudosound velocity component $u^{cs}$ at $\mathrm{Re}_\lambda \approx 180$. Based on the definition of the pseudosound velocity, there is a single scaling of $M_t^4$ for $K^{cs}/K^s$. At a fixed Taylor Reynolds number, as the turbulent Mach number decreases to zero, the curve for $K^c/K^s$ approaches the curve of $K^{cs}/K^s$. We infer that as the turbulent Mach number becomes infinitesimal, the compressible velocity component satisfies the pseudosound relationship [17].

As the turbulent Mach number increases, the ratio $K^c/K^s$ deviates from the pseudosound constitutive relationship and the compressible fields are dominated by the acoustic modes for $M_t > 0.1$. The normalized energy $K^c/K^s$ of the compressible velocity shows a very steep increase with the increase in turbulent Mach number in the range of $0.1 \leqslant M_t \leqslant 0.4$. Another transition occurs at $M_t = 0.4$, after which, $K^c/K^s$ increases more slowly with turbulent Mach number, at approximately the rate of $M_t^2$. Our observations are consistent with a previous study by Jagannathan

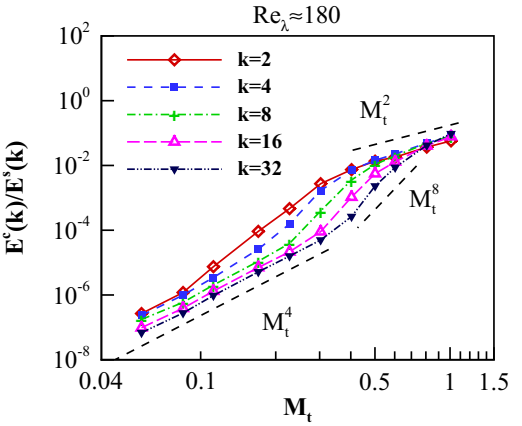


FIG. 12. Normalized spectrum of the compressible velocity component $E^c(k)/E^s(k)$ at $\mathrm{Re}_\lambda \approx 180$.

and Donzis [9]. In their work, they suggested two different scaling ranges: a $M_t^4$ scaling for small turbulent Mach numbers and a $M_t^2$ scaling for larger turbulent Mach numbers. For the small turbulent Mach number $M_t \leqslant 0.1$, an improved version of EDQNM model proposed by Fauchet and Bertoglio [27] suggested the $M_t^4$ scaling of $K^c/K^s$. Additionally, the $M_t^4$ scaling of $K^c/K^s$ is a result of the pseudosound relationship suggested by Ristorcelli [17].

Moreover, we study the turbulent Mach number dependence of the normalized spectrum of the compressible velocity component $E^c(k)/E^s(k)$ as shown in Fig. 12. In this figure, we plot the ratio of the spectrum $E^c(k)/E^s(k)$ at a grid resolution of $512^3$ where the Taylor Reynolds number $\mathrm{Re}_\lambda$ is approximately 180. For small wave numbers, the $M_t$ dependence behavior of $E^c(k)/E^s(k)$ is similar to that of $K^c/K^s$. There are more interesting observations for larger wave numbers. As wave number $k$ increases, the $M_t^4$ scaling occurs in a wider range of $M_t$. Particularly, there is a $M_t^4$ scaling in the range of $M_t \leqslant 0.3$ for $k = 32$. The transition to the region of $M_t^2$ scaling delays when $k$ increases. The observations suggest that acoustic waves are harder to generate at smaller scales. Between two regions of $M_t^4$ and $M_t^2$ scaling, approximately, there is a transitional $M_t^8$ scaling region for the inertial range of wave numbers $8 \leqslant k \leqslant 32$.

Similar to the decomposition of velocity field, the decomposition of the dissipation rate of the kinetic energy per unit mass is given by $\epsilon = \epsilon^s + \epsilon^c$, where the solenoidal component is $\epsilon^s = \langle \mu/(\mathrm{Re}\rho)\rangle\langle\omega_i\omega_i\rangle$ and the compressible component is $\epsilon^c = \langle 4\mu/(3\mathrm{Re}\rho)\rangle\langle\theta^2\rangle$ [9]. Here, $\omega_i = \epsilon_{ijk}\partial u_j/\partial x_k$ is the vorticity. We present the normalized compressible dissipation rate $\epsilon^c/\epsilon^s$ of velocity in Fig. 13. It is shown that for a small turbulent Mach number $M_t \leqslant 0.2$, there is a $M_t^4$ scaling relation. For higher turbulent Mach numbers in the range of $0.4 \leqslant M_t \leqslant 1.0$, $\epsilon^c/\epsilon^s$ has a $M_t^5$ scaling. Recent direct numerical simulations by Jagannathan and Donzis [9] suggested a power law scaling of $M_t^{4.1}$ for $\epsilon^c/\epsilon^s$ at $M_t \geqslant 0.3$. For a low turbulent Mach number, the scaling $M_t^4$ has been proposed by Ristorcelli [17] using pseudosound constitutive analysis and by Fauchet and Bertoglio [1,27] using an improved version of the EDQNM model. For moderate to high turbulent Mach numbers, an EDQNM model reveals a $M_t^5$ scaling dependence of $\epsilon^c/\epsilon^s$ [1]. Our numerical simulations are in agreement with the theoretical prediction.

It is remarkable that at a low turbulent Mach number, the normalized dissipation rate $\epsilon^c/\epsilon^s$ depends on the Reynolds number. For a given low turbulent Mach number, $\epsilon^c/\epsilon^s$ will decreases with an increase in the Taylor Reynolds number. By the pseudosound constitutive relation [17] and Kolmogorov turbulence theory, the spectrum of the compressible dissipation in the inertial range $(1/L_I < k < 1/\eta)$ can be determined by the spectrum of the pseudosound component of the velocity [Eq. (36)]:

$$E^{cs}_{\mathrm{dissipation}}(k) = \tfrac{8}{3}\nu k^2 E^{cs}(k) = \tfrac{8}{3}\nu C_v^{PS} M_t^4 L_I^{-4/3}\epsilon^{2/3}k^{-1}. \tag{44}$$

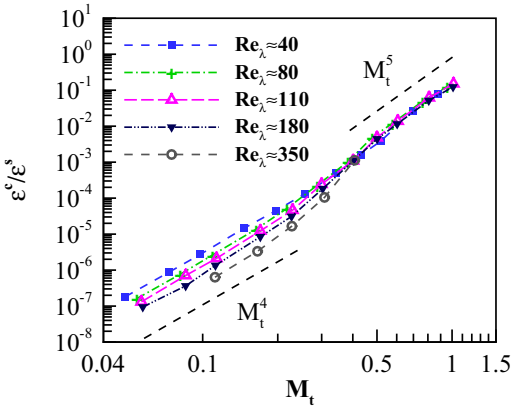


FIG. 13. Normalized dissipation of the compressible velocity component $\epsilon^c/\epsilon^s$.

Therefore, by integration of the dissipation spectrum $\epsilon^c = \epsilon^{cs} \approx \int_{1/L_I}^{1/\eta} E^{cs}_{\text{dissipation}}(k)\, dk$, we obtain the following scaling relation:

$$\epsilon^c/\epsilon^s \sim M_t^4 \mathrm{Re}_L^{-1} \log(\mathrm{Re}_L), \tag{45}$$

where $\mathrm{Re}_L = u^{\mathrm{rms}} L_I/\nu$ is the Reynolds number based on the integral scale. The theoretical scaling (45) is consistent with an EDQNM model [1,27]. In numerical simulations of isotropic turbulence, we usually consider $\mathrm{Re}_\lambda$ instead of $\mathrm{Re}_L$. The relation between $\mathrm{Re}_\lambda$ and $\mathrm{Re}_L$ is [35] $\mathrm{Re}_\lambda \sim \mathrm{Re}_L^{1/2}$, which has been verified in weakly compressible isotropic turbulence [9]. Thus, we obtain the scaling relation

$$\epsilon^c/\epsilon^s \sim M_t^4 \mathrm{Re}_\lambda^{-2} \log(\mathrm{Re}_\lambda). \tag{46}$$

From Fig. 14, we show that in numerical simulations $\mathrm{Re}_\lambda \approx 350$ is not high enough for the appearance of the $M_t^4 \mathrm{Re}_\lambda^{-2} \log(\mathrm{Re}_\lambda)$ scaling.

### B. Mach number scaling of pressure, density, and temperature

Now we begin to consider the rms values of pressure, density, and temperature in simulated compressible turbulent flows. We plot the normalized rms values of pressure and its two components,

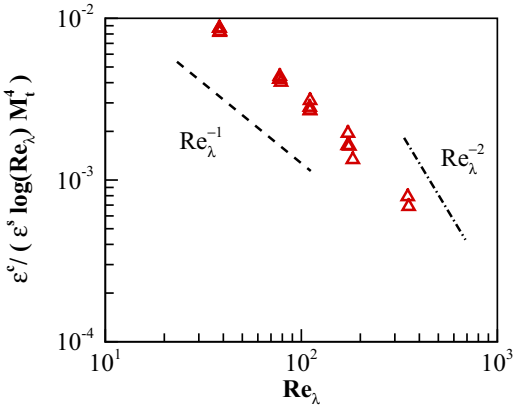


FIG. 14. Normalized dissipation of the compressible velocity component $\epsilon^c/(\epsilon^s \log(\mathrm{Re}_\lambda) M_t^4)$ as function of $\mathrm{Re}_\lambda$, at $M_t \leqslant 0.2$.

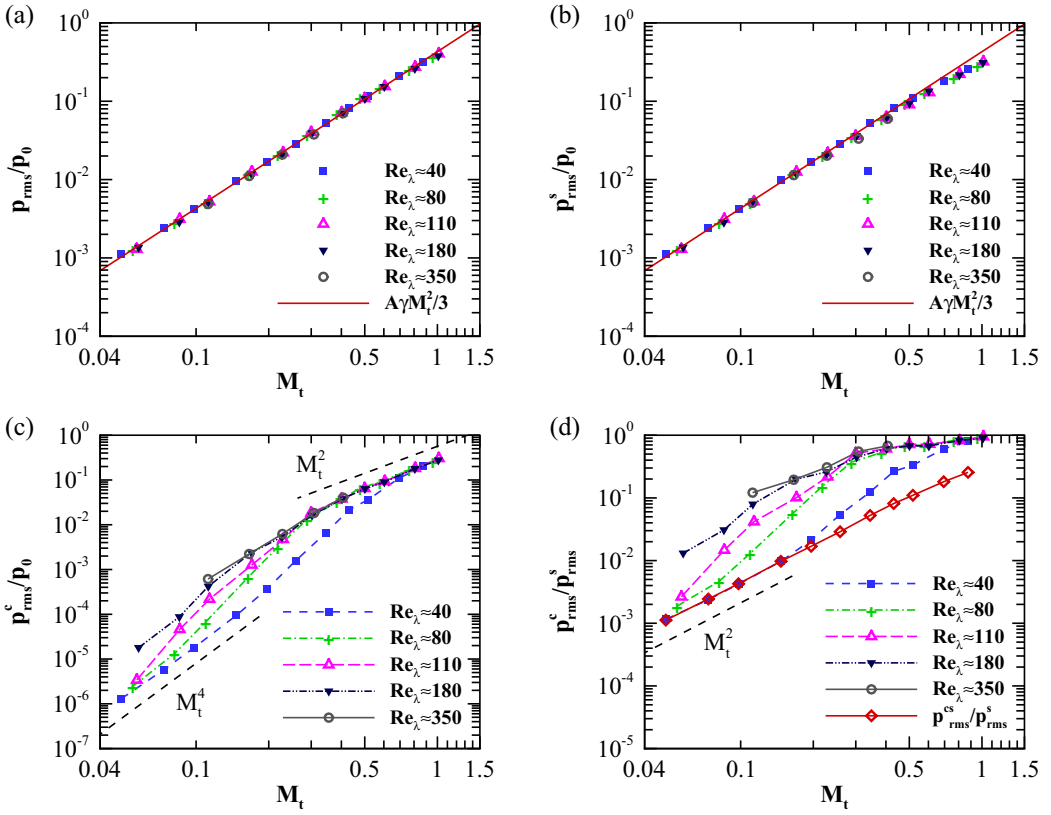


FIG. 15. Normalized rms values of pressure, solenoidal pressure component and compressible pressure component at different turbulent Mach numbers $M_t$ and different Taylor Reynolds numbers $\mathrm{Re}_\lambda$. The solid lines in (a) and (b) represent $A\gamma M_t^2/3$ where $A = 0.92$. The ratio $p^{cs}_{\mathrm{rms}}/p^s_{\mathrm{rms}}$ at $\mathrm{Re}_\lambda \approx 180$ is also plotted in (d).

$p_{\mathrm{rms}}/p_0$, $p^s_{\mathrm{rms}}/p_0$, and $p^c_{\mathrm{rms}}/p_0$, in Fig. 15. It is well known that in incompressible turbulence, the rms value of pressure has the following relation: $p_{\mathrm{rms}} = \sqrt{\langle (p - p_0)^2 \rangle} \approx A\rho_0 u'^2/3$, where $u' = \sqrt{\langle u_1^2 + u_2^2 + u_3^2 \rangle}$ and $A = 0.92$ [45]. We note that $u'^2 \approx M_t^2 \gamma p_0/\rho_0$. Thus, we can obtain the following relation for the normalized rms value of pressure in compressible turbulence:

$$p_{\mathrm{rms}}/p_0 \approx \frac{A\gamma}{3} M_t^2. \tag{47}$$

We show that the solid lines in Figs. 15(a) and 15(b) almost overlap with the numerical data at different Taylor Reynolds numbers and turbulent Mach numbers, indicating that the numerical results are in good agreement with the $M_t^2$ scaling relation (47). The rms value of the solenoidal pressure $p^s_{\mathrm{rms}}/p_0$ is almost identical to the rms value of pressure $p_{\mathrm{rms}}/p_0$ at relatively small turbulent Mach numbers $M_t \leqslant 0.4$. Thus, we have verified the relation (47) in the numerical simulations of compressible turbulence, which is consistent with the situation of incompressible turbulence. In a previous study, Donzis and Jagannathan reported a slightly larger coefficient $A = 1.2$ in compressible turbulence [24].

From Fig. 15(c), we find that the compressible component $p^c_{\mathrm{rms}}/p_0$ is dependent on both turbulent Mach number $M_t$ and Taylor Reynolds number $\mathrm{Re}_\lambda$. At small turbulent Mach numbers $M_t \leqslant 0.4$, the value $p^c_{\mathrm{rms}}/p_0$ increases with the increase in the Taylor Reynolds number $\mathrm{Re}_\lambda$, similar to the behavior of the normalized energy of the compressible velocity $K^c/K^s$. At relatively high turbulent Mach numbers $M_t \geqslant 0.5$, we identify a $M_t^2$ scaling behavior of $p^c_{\mathrm{rms}}/p_0$, which is similar to $p^s_{\mathrm{rms}}/p_0$.

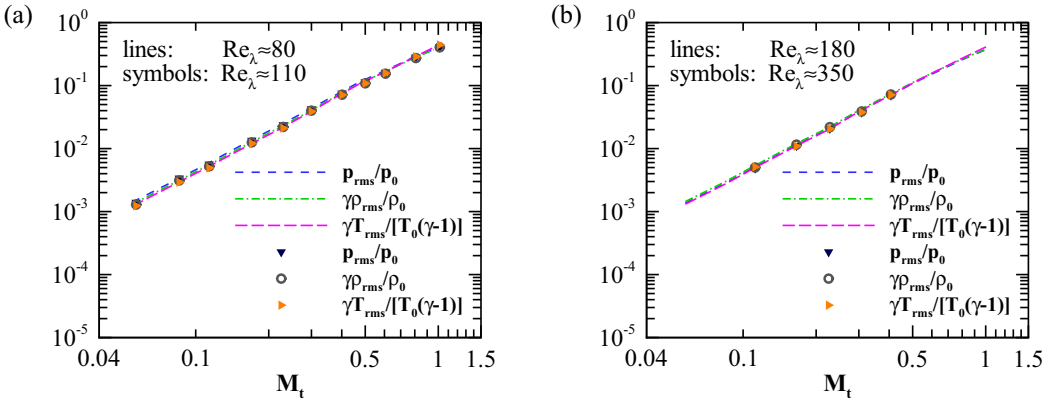


FIG. 16. Normalized rms values of pressure, density, and temperature at different turbulent Mach numbers $M_t$ and different Taylor Reynolds numbers $\mathrm{Re}_\lambda$.

Previously, Jagannathan and Donzis reported a $M_t^2$ scaling behavior of $p^c_{\mathrm{rms}}/p_0$ at $0.3 \leqslant M_t \leqslant 0.6$ and a $M_t^2$ scaling behavior of $p^s_{\mathrm{rms}}/p_0$ at $0.1 \leqslant M_t \leqslant 0.6$ [24].

At $\mathrm{Re}_\lambda \approx 40$, we also observe the purely pseudosound scaling relation $p^c_{\mathrm{rms}}/p_0 \sim M_t^4$ for $M_t \leqslant 0.1$. The purely pseudosound regime of the compressible pressure is further confirmed in Fig. 15(d). At $\mathrm{Re}_\lambda \approx 40$ and $M_t \leqslant 0.1$, the ratio $p^c_{\mathrm{rms}}/p^s_{\mathrm{rms}}$ is identical to the ratio $p^{cs}_{\mathrm{rms}}/p^s_{\mathrm{rms}}$, which exhibits the following scaling behavior: $p^c_{\mathrm{rms}}/p^s_{\mathrm{rms}} \sim M_t^2$. Due to the limitation of computational resource, we cannot perform numerical simulation at very small turbulent Mach numbers and cannot observe the pseudosound scaling of the compressible pressure at relatively high Taylor Reynolds numbers $\mathrm{Re}_\lambda \geqslant 80$. We infer that for a fixed Taylor Reynolds number $\mathrm{Re}_\lambda$, the pseudosound scaling relation will appear as the turbulent Mach number $M_t$ becomes very small.

In Fig. 15(d), we show that the ratio $p^c_{\mathrm{rms}}/p^s_{\mathrm{rms}}$ is quite small at small turbulent Mach numbers $M_t \leqslant 0.4$, indicating that the solenoidal pressure component is predominant over the compressible component. At relatively high turbulent Mach numbers $M_t \geqslant 0.4$ and high Taylor Reynolds numbers $\mathrm{Re}_\lambda \geqslant 80$, the values of $p^c_{\mathrm{rms}}/p^s_{\mathrm{rms}}$ are close to 1.0, indicating that the solenoidal and compressible components are of the same order of magnitude. Our numerical results of $p^c_{\mathrm{rms}}/p^s_{\mathrm{rms}}$ are consistent with the previous results given by Jagannathan and Donzis. They showed that the values $p^c_{\mathrm{rms}}/p^s_{\mathrm{rms}}$ are between 0.1 and 2.0 at $0.1 \leqslant M_t \leqslant 0.6$ and increases with the increase in the turbulent Mach number [24].

We plot the normalized rms values of pressure, density, and temperature, $p_{\mathrm{rms}}/p_0$, $\gamma\rho_{\mathrm{rms}}/\rho_0$, and $\gamma T_{\mathrm{rms}}/[(\gamma-1)T_0]$, at different turbulent Mach numbers $M_t$ and different Taylor Reynolds numbers $\mathrm{Re}_\lambda$ in Fig. 16. Here, $\rho_{\mathrm{rms}} = \sqrt{\langle(\rho-\rho_0)^2\rangle}$ and $T_{\mathrm{rms}} = \sqrt{\langle(T-T_0)^2\rangle}$. The factors $\gamma$ and $\gamma/(\gamma-1)$ are determined based on the isentropic relations: $\gamma\rho'/\rho_0 = p'/p_0$ and $[\gamma/(\gamma-1)]T'/T_0 = p'/p_0$. We show that the normalized rms values of pressure, density, and temperature overlap with one another, and they exhibit a $M_t^2$ scaling behavior. Therefore, from Eq. (47) we obtain the following relations for the normalized rms values of density and temperature:

$$\rho_{\mathrm{rms}}/\rho_0 \approx \frac{A}{3}M_t^2, \tag{48}$$

$$T_{\mathrm{rms}}/T_0 \approx \frac{A(\gamma-1)}{3}M_t^2, \tag{49}$$

where $A = 0.92$.

## VII. SUMMARY AND CONCLUSIONS

In this paper, we investigated the spectra and statistics of velocity and thermodynamic variables by numerical simulations of solenoidally forced stationary compressible isotropic turbulence. We introduced a decomposition of the compressible velocity component and compressible pressure component. The compressible field has been decomposed into a pseudosound component and an acoustic component. At a given Taylor Reynolds number, the pseudosound mode will finally dominate in compressible turbulence as the turbulent Mach number becomes infinitesimal. We also proposed some theoretical arguments to address the inertial statistics of the compressible field in the fully developed weakly compressible turbulence: The spectrum of the compressible velocity component $E^c(k)$ exhibits a $M_t^4 k^{-3}$ scaling and the spectrum of the compressible pressure component $E_p^c(k)$ exhibits a $M_t^4 k^{-11/3}$ scaling, in the inertial range, at the zero turbulent Mach number limit.

In our numerical simulations, for the simulated stationary weakly compressible turbulence at turbulent Mach numbers $M_t \leqslant 0.4$, there is not a single scaling relation of the spectrum of the compressible velocity component in the convective inertial range of incompressible velocity. We observed a transition between the pseudosound-mode-dominated region and the acoustic-mode-dominated region. We identified a critical wave number $k_c$: The pseudosound mode dominates at $k \geqslant k_c$ and the acoustic mode dominates at $k \leqslant k_c$.

We showed that the spectra of pressure, density, and temperature exhibit a $k^{-7/3}$ scaling in the inertial range at low turbulent Mach numbers $M_t \leqslant 0.3$, which is similar to the pressure spectrum in incompressible turbulence. We also presented that the spectra of pressure, density, and temperature exhibit a $k^{-5/3}$ scaling in the inertial range at high turbulent Mach numbers $M_t \geqslant 0.5$.

We also found a number of turbulent Mach number scaling behaviors of the compressible velocity component in our numerical simulations. The energy $K^c$ of the compressible velocity component has a $M_t^4$ scaling at low turbulent Mach numbers $M_t \leqslant 0.1$. $K^c$ exhibits approximately a $M_t^2$ scaling at high turbulent Mach numbers $M_t \geqslant 0.4$ and at moderate Taylor Reynolds numbers $\mathrm{Re}_\lambda \geqslant 80$. We showed that the dissipation rate of the compressible velocity component has a $\epsilon^c \sim M_t^4 \mathrm{Re}_L^{-1} \log(\mathrm{Re}_L)$ scaling at the zero turbulent Mach number limit. Moreover, we reported that the normalized rms values of pressure, density, and temperature exhibit a $M_t^2$ scaling behavior at turbulent Mach numbers $0.05 \leqslant M_t \leqslant 1.0$ in numerical simulations.

Finally, we emphasize that numerical simulations at higher grid resolutions are required to eliminate the low Reynolds number effect on the spectrum of compressible velocity. The one-point statistics and spectra of compressible isotropic turbulence have been studied for purely solenoidal forcing in this paper. The effect of large-scale compressible forcing on the one-point statistics and spectra remains to be further investigated.

## ACKNOWLEDGMENTS

The authors gratefully acknowledge the valuable discussions with Dr. Jingyuan Yang, Dr. Yantao Yang, and Professor Shiyi Chen. The authors also appreciate the valuable comments by the anonymous referee. The numerical simulations were done on the supercomputer at Nagoya University. The work of T.G. and T.W. were supported by JSPS KAKENHI Grant Numbers 15H02218 and 26420106, respectively. J.W. acknowledges Dr. Izumi Saito for much help using the supercomputer at Nagoya University.

[1] P. Sagaut and C. Cambon, *Homogeneous Turbulence Dynamics* (Cambridge University Press, Cambridge, UK, 2008).

[2] J. Cardy, G. Falkovich, and K. Gawedzki, *Non-equilibrium Statistical Mechanics and Turbulence* (Cambridge University Press, Cambridge, UK, 2008).

[3] R. Samtaney, D. I. Pullin, and B. Kosovic, Direct numerical simulation of decaying compressible turbulence and shocklet statistics, Phys. Fluids **13**, 1415 (2001).

[4] S. Pirozzoli and F. Grasso, Direct numerical simulations of isotropic compressible turbulence: Influence of compressibility on dynamics and structures, Phys. Fluids **16**, 4386 (2004).
[5] H. Aluie, Compressible Turbulence: The Cascade and its Locality, Phys. Rev. Lett. **106**, 174502 (2011).
[6] S. Galtier and S. Banerjee, Exact Relation for Correlation Functions in Compressible Isothermal Turbulence, Phys. Rev. Lett. **107**, 134501 (2011).
[7] J. Wang, Y. Yang, Y. Shi, Z. Xiao, X. He, and S. Chen, Cascade of Kinetic Energy in Three-Dimensional Compressible Turbulence, Phys. Rev. Lett. **110**, 214505 (2013).
[8] A. G. Kritsuk, R. Wagner, and M. L. Norman, Energy cascade and scaling in supersonic isothermal turbulence, J. Fluid Mech. **729**, R1 (2013).
[9] S. Jagannathan and D. A. Donzis, Reynolds and Mach number scaling in solenoidally-forced compressible turbulence using high-resolution direct numerical simulations, J. Fluid Mech. **789**, 669 (2016).
[10] J.-Z. Zhu, Isotropic polarization of compressible flows, J. Fluid Mech. **787**, 440 (2016).
[11] L. S. G. Kovasznay, Turbulence in supersonic flow, J. Aeronaut. Sci. **20**, 657 (1953).
[12] R. Benzi, L. Biferale, R. T. Fisher, L. P. Kadanoff, D. Q. Lamb, and F. Toschi, Intermittency and Universality in Fully Developed Inviscid and Weakly Compressible Turbulent Flows, Phys. Rev. Lett. **100**, 234503 (2008).
[13] J. Wang, Y. Shi, L.-P. Wang, Z. Xiao, X. T. He, and S. Chen, Effect of shocklets on the velocity gradients in highly compressible isotropic turbulence, Phys. Fluids **23**, 125103 (2011).
[14] J. Wang, Y. Shi, L.-P. Wang, Z. Xiao, X. T. He, and S. Chen, Effect of compressibility on the small scale structures in isotropic turbulence, J. Fluid Mech. **713**, 588 (2012).
[15] J. Wang, Y. Shi, L.-P. Wang, Z. Xiao, X. T. He, and S. Chen, Scaling and Statistics in Three-Dimensional Compressible Turbulence, Phys. Rev. Lett. **108**, 214505 (2012).
[16] S. Sarkar, G. Erlebacher, M. Y. Hussaini, and H. O. Kreiss, The analysis and modeling of dilatational terms in compressible turbulence, J. Fluid Mech. **227**, 473 (1991).
[17] J. R. Ristorcelli, A pseudo-sound constitutive relationship for the dilatational covariances in compressible turbulence, J. Fluid Mech. **347**, 37 (1997).
[18] M. J. Lighthill, On sound generated aerodynamically, I: General theory, Proc. R. Soc. London, Ser. A **211**, 564 (1952).
[19] G. Erlebacher, M. Y. Hussaini, H. O. Kreiss, and S. Sarkar, The analysis and simulation of compressible turbulence, Theoret. Comput. Fluid Dynamics **2**, 73 (1990).
[20] S. Kida and S. A. Orszag, Energy and spectral dynamics in forced compressible turbulence, J. Sci. Comput. **5**, 85 (1990).
[21] H. Miura and S. Kida, Acoustic energy exchange in compressible turbulence, Phys. Fluids **7**, 1732 (1995).
[22] D. Li, X. Zhang, and G. He, Temporal decorrelations in compressible isotropic turbulence, Phys. Rev. E **88**, 021001(R) (2013).
[23] M. R. Petersen and D. Livescu, Forcing for statistically stationary compressible isotropic turbulence, Phys. Fluids **22**, 116101 (2010).
[24] D. A. Donzis and S. Jagannathan, Fluctuations of thermodynamic variables in stationary compressible turbulence, J. Fluid Mech. **733**, 221 (2013).
[25] F. Bataille, Y. Zhou, and J. P. Bertoglio, Energy transfer and triadic interactions in compressible turbulence, Tech. Rep. Defense Technical Information Center Document, 1997 (unpublished).
[26] J. P. Bertoglio, F. Bataille, and J. D. Marion, Two-point closures for weakly compressible turbulence, Phys. Fluids **3**, 290 (2001).
[27] G. Fauchet and J. P. Bertoglio, An analytical expression for the spectrum of compressible turbulence in the low Mach number limit, in *Advances in Turbulence VII*, edited by U. Frisch, Fluid Mechanics and Its Applications Vol. 46 (Springer Science+Business Media B.V., Dordrecht, Netherlands, 1998), p. 317.
[28] J. Wang, L.-P. Wang, Z. Xiao, Y. Shi, and S. Chen, A hybrid numerical simulation of isotropic compressible turbulence, J. Comp. Phys. **229**, 5257 (2010).
[29] G. P. Zank and W. H. Matthaeus, The equations of nearly incompressible fluids, I: Hydrodynamics, turbulence, and waves, Phys. Fluids A **3**, 69 (1991).
[30] T. Colonius, S. K. Lele, and P. Moin, Sound generation in a mixing layer, J. Fluid Mech. **330**, 375 (1997).
[31] C. K. W. Tam and L. Auriault, Jet mixing noise from fine-scale turbulence, AIAA J. **37**, 145 (1999).

[32] M. Wang, J. B. Freund, and S. K. Lele, Computational prediction of flow-generated sound, Annu. Rev. Fluid Mech. **38**, 483 (2006).
[33] A. N. Kolmogorov, The local structure of turbulence in incompressible viscous fluid for very large Reynolds numbers, Proc. R. Soc. London, Ser. A **434**, 9 (1991).
[34] U. Frisch, *Turbulence: The Legacy of A. N. Kolmogorov* (Cambridge University Press, Cambridge, UK, 1995).
[35] S. B. Pope, *Turbulent Flows* (Cambridge University Press, Cambridge, UK, 2000).
[36] S. K. Lele, Compact finite difference schemes with spectral-like resolution, J. Comput. Phys. **103**, 16 (1992).
[37] D. S. Balsara and C. W. Shu, Monotonicity preserving weighted essentially non-oscillatory schemes with increasingly high order of accuracy, J. Comput. Phys. **160**, 405 (2000).
[38] T. Watanabe and T. Gotoh, Inertial-range intermittency and accuracy of direct numerical simulation for turbulence and passive scalar turbulence, J. Fluid Mech. **590**, 117 (2007).
[39] T. Ishihara, Y. Kaneda, M. Yokokawa, K. Itakura, and A. Uno, Small-scale statistics in high-resolution direct numerical simulation of turbulence: Reynolds number dependence of one-point velocity gradient statistics, J. Fluid Mech. **592**, 335 (2007).
[40] D. A. Donzis, K. R. Sreenivasan, and P. K. Yeung, Scalar dissipation rate and dissipative anomaly in isotropic turbulence, J. Fluid Mech. **532**, 199 (2005).
[41] T. Ishihara, T. Gotoh, and Y. Kaneda, Study of high-Reynolds number isotropic turbulence by direct numerical simulation, Annu. Rev. Fluid Mech. **41**, 165 (2009).
[42] T. Watanabe and T. Gotoh, Statistics of a passive scalar in homogeneous turbulence, New J. Phys. **6**, 40 (2004).
[43] T. Gotoh and D. Fukayama, Pressure Spectrum in Homogeneous Turbulence, Phys. Rev. Lett. **86**, 3775 (2001).
[44] Y. Tsuji and T. Ishihara, Similarity scaling of pressure fluctuation in turbulence, Phys. Rev. E **68**, 026309 (2003).
[45] D. A. Donzis, K. R. Sreenivasan, and P. K. Yeung, Some results on the Reynolds number scaling of pressure statistics in isotropic turbulence, Physica D (Amsterdam, Neth.) **241**, 164 (2012).